Inhibitory synaptic plasticity and gain modulation in cerebellar nucleus neurons

Dimitris Bampasakis

January 2015

Submitted to the University of Hertfordshire in partial fulfilment
of the requirements of the degree of

Doctor of Philosophy

Στη Μαρία

Contents

6

List of Figures

7

List of Tables

Nomenclature

A amplitude of synaptic response.

A_0 initial amplitude of synaptic response.

AP   action potential.

C_m membrane capacitance per unit area in [F/cm^2].

c_m membrane capacitance per unit length in [F/cm].

D STD depression factor.

δ STD scaling factor.

$Diam$ Compartmental diameter.

E_K potassium reversal potential in [V].

E_L leak reversal potential in [V].

E_{Na} sodium reversal potential in [V].

EPSC   ecxitatory postsynaptic current.

E_r resting membrane voltage.

Fac STD facilitation factor.

g_K potassium conductanc in [S].

g_L leak conductanc in [S].

G_m membrane conductance per unit area in [S/cm^2]. 43

g_m membrane conductance per unit length in [S/cm]. 43

g_{Na} sodium conductanc in [S]. 45

i_i intracellular current in [A]. 42

I_K potassium current in [A]. 42

I_L leakage current in [A]. 42

i_m membrane current density in [A/cm]. 42

I_{Na} sodium current in [A]. 42

IPSC   inhibitory postsynaptic current. 50

ISI   inter-spike interval(ISI) is the time between two sunsequent APs 52

L Compartmental length. 62

PSC   postsynaptic current. 50

r_i intracellular resistivity per unit length in [Ω/cm]. 42

R_m membrane resistance times unit area in [Ω/cm^2]. 43

r_m membrane resistance times unit length in [Ω/cm]. 43

τ_m passive membrane time constant. 43

V_e resting membrane voltage. 41

V_i resting membrane voltage. 41

E_{syn} synaptic reversal potential. 50

f_c input frequancy, when there is no variability in ISI 52

$\bar{g}_{syn}$ maximum postsynaptic conductance. 50

G_{exc} see G_{syn}. 52

g_{exc} see g_{syn}. 50

G_{inh} see G_{syn}. 52

g_{inh} see g_{syn}. 50

G_{syn} Average synaptic conductance. Can also be G_{exc} or G_{inh} in case of an excitatory or an inhibitory conductance, respectively. 52

g_{syn} synaptic conductance. Can also be g_{exc} or g_{inh} in case of an excitatory or an inhibitory conductance, respectively. 50

R_{ss} steady state level of the pre-synaptic release probability. 56

R   pre-synaptic release probability 56

t_s time of AP's arrival. 50

V   Voltage difference across the membrane 50

τ time constant of depression. 56

τ_1 decay time constant. 50

τ_2 rise time constant. 50

Acknowledgements

It has been almost ten year since I first decided to undertake a PhD, while still doing my bachelor studies in Physics, at the University of Crete. Writing these lines, and having only minor details for the rest of my thesis to complete, I look back and realize the support I received during my scientific endeavours. There are many people I want to thank, family, friends, and colleagues, who supported me throughout the years, and enabled me to fulfil my aspirations.

First and foremost I want to thank my parents. Ever since I was young I received their undivided attention and support. Through good and bad times, they have always been there to support and guide me. Without their help, I would not have reached this far.

For the scientific part, however, I am indebted to Dr Volker Steuber, Dr Neil Davey and Dr Reinoud Maex. Their help during my PhD was vast, contributing not only to the scientific content, and providing career and development advice, but also catering to personal needs and caring for my well-being. I feel grateful for the treatment I received, and I really can not thank them enough. These feelings extend to the University of Hertfordshire that provided financial support, excellent facilities, and an outstanding postgraduate course.

I would also like to thank the staff of the interdisciplinary MSc programme I attended in Crete, where I had the opportunity to study Brain and Mind sciences. The knowledge I acquired during the course helped not only in getting accepted for a PhD, but it also gave me a great insight that

helped me during my studies. Special thanks to Dr Stathis Kasderidis, who supervised me during my BSc final year project.

Last, but most importantly, words can not express my gratitude towards my wife, Maria. For more than ten years, she has encouraged and support me. This thesis is dedicated to her.

Abstract

Neurons can encode information using the rate of their action potentials, making the relation between input rate and output rate a prominent feature of neuronal information processing. This relation, known as I–O function, can rapidly change in response to various factors or neuronal processes. Most noticeably, a neuron can undergo a multiplicative operation, resulting in a change of the slope of its I–O curve, also know as gain change.

Gain changes represent multiplicative operations, and they are widespread. They have been found to play an important role in the encoding of spatial location and coordinate transformation, to signal amplification, and other neuronal functions. One of the factors found to introduce and control neuronal gain is synaptic Short Term Depression (STD).

We use both integrate-and-fire and conductance based neuron models to identify the effect of STD in excitatory and inhibitory modulatory input. More specifically, we are interested in the effect of STD at the inhibitory synapse from Purkinje cells to cerebellar nucleus neurons. Using a previously published, biologically realistic model, we find that the presence of STD results in a gain change. Most importantly we identify STD at the inhibitory synapse to enable excitation-mediated gain control.

To isolate the mechanism that allows excitation to control gain, even though STD is applied at a different synapse, we first show that the overall effect is mediated by average conductance. Having done this, we find that the effect of STD is based on the non-linearity introduced in the relation between input rate and average conductance. We find this effect to vary, depending

on the position of the I–O function on the input rate axis. Modulatory input shifts the I–O curve along the input rate axis, consequently shifting it to a position where STD has a different effect. The gain differences in the STD effects between the two positions enable excitation to perform gain control.

1

Introduction

1.1 Motivation

Our perception of everyday reality, along with our thoughts and functions, rely on the encoding, processing and transmission of information through neuronal pathways. As the result of evolution through millions of years, neuronal morphology, biophysics and connectivity is diverse; despite the preservation of some characteristics since long before man stepped on the planet (Billings et al., 2014).

Being so diverse, neuronal functions are difficult to understand as a whole, so one should take the reductionist approach; or as Harry Grundfest had put it: "To understand mind we needed to look at the brain one cell at a time" (Kandel, 2007). In this fashion, to understand gain modulation we focus on a cerebellar nucleus neuron.

Gain modulation refers to a change of the slope of a neuron's I–O function, that is, the output firing rate as a function of input rate. This slope change can result from various mechanisms, and it is used by the brain in functions of various complexities, like the improvement of information transmission (Brenner et al., 2000), and the coordinate transformation from the retina coordinate system to the body coordinate system (Zipser and Andersen, 1988). Here, we are interested in gain modulation arising from the introduction of short-term synaptic depression (STD).

Synaptic depression has already be studied at the excitatory synapse from mossy fibres to granule cells, and it is known to enable neuronal gain control (Rothman et al., 2009). What we are interested in, is the effect of

STD when present at inhibitory synapses, and in particular at the inhibitory synapse between Purkinje cells (PCs) and cerebellar nucleus (CN) neurons.

1.2   Aim of Thesis

The aim of this thesis is to advance our understanding of how STD can contribute to gain modulation, and in particular to identify the effect that STD at inhibitory synapses has. To do so we work with neuronal models of various complexity.

We start by replicating previous findings (Rothman et al., 2009) that look at the effect of STD at the excitatory synapse from mossy fibres to granule cells. To do so, we use an integrate-and-fire neuron to simulate the effect of STD at an excitatory synapse, and identify the resulting gain changes. Since STD is applied at the excitatory synapse it is expected to induce gain changes in the output rate as a function of excitatory input. What is more interesting however, is how STD at the excitatory synapse can enable inhibitory conductances to perform gain control, an effect evident in our simulation data.

To identify the effect of STD at inhibitory synapses, we used a biologically realistic, conductance based model of a cerebellar nucleus neuron. The input that cerebellar nucleus neurons receive comes from Purkinje cells and exhibits STD, making them fit for the study of STD at this inhibitory synapse. But CN neurons receive both inhibitory and excitatory input. This makes them ideal for studying the effect that STD at the inhibitory synapse will have on the operation performed by excitatory input. This is intriguing since STD at one synapse can affect the operation performed by a different synapse.

Our approach is to use an already published model of a cerebellar nucleus neuron (Steuber et al., 2011) to identify the role of STD. Apart from quantifying the effect of STD however, it is also important to understand the mechanisms that underlie it. After addressing "what"; "how" is the second question that must be answered. This is why we try to elucidate the mechanism responsible for enabling gain control.

1.3 Contribution to knowledge

The research presented here describes, and hopefully elucidates, the effect that STD at the inhibitory synapse between Purkinje cells and cerebellar nucleus neurons has on the output of a cerebellar nucleus neuron. Our research was limited to simulating model neurons, but our use of previously published biologically realistic models of cerebellar nucleus neurons capable of replicating in vitro data, along with the use of integrate-and-fire models illustrating that the effects are persistent across different modalities, increases our confidence in our results. Our work has resulted in four distinctive findings. More specifically

- We discover the effect of STD at an inhibitory synapse, showing that STD performs a gain change, and that it enables excitation-mediated gain modulation.

- We show that the effect of STD on the gain change is a robust phenomenon and that it persists in the presence of different degrees of input synchronicity and regularity, and for different STD levels.

- We identify the underlying transformation and explain how changes in the synapse map to changes in the I–O function.

- We explain how gain modulation arises; using the already identified transformation, we show how STD can lead to gain changes.

1.4 Overview of thesis

The rest of this document is divided into six chapters. These chapters, and a summary of their content, are given below.

chapter 2 **Gain modulation:** Gain modulation is a prominent function in neuronal computation. From the encoding of spatial location, and coordinate transformation, to signal amplification and prevention of firing saturation, along with a number of mechanism responsible for changes in neuronal gain, gain control seems to play a key role in neuronal processing. In this chapter we define gain modulation, and move on to discuss various roles of gain modulations, along with some of the mechanisms responsible for gain control.

chapter 3 **Computational neuroscience:** To investigate neuronal gain, and to understand how the mechanisms responsible for gain control work, it is necessary to use computational models. To model gain modulation, one must build on simple models that describe how currents flow inside a neuron, and how they flow across its membrane. Although these models are provided by modern simulation environments such as NEURON (Carnevale T. and Hines L., 2006) and GENESIS (Bower and Beeman, 2014), they are the core of computational neuroscience. Thus in chapter 3 we discuss some of the most important theories of computational neuroscience, like Cable Theory, and the Hodgkin-Huxley model, along with a number of STD models.

chapter 4 **Effect of STD at excitatory synapses:** In this chapter we use an integrate-and-fire neuron, receiving both excitatory and inhibitory input. We simulate this neuron in the presence and absence of STD at the excitatory synapse to demonstrate how STD at the excitatory synapse can change the gain, and allow inhibition to control the gain.

chapter 5 **Effects of STD at an inhibitory synapse:** To investigate the effect of STD at inhibitory synapses, we use a biologically realistic model of a cerebellar nucleus neuron. Performing simulations in the presence and absence of STD we find the effect of STD to be similar to the one found in the previous chapter. We discuss these effects, and show how both the post-synaptic conductance and the I–O function undergo the same transformation. We proceed to explain how this transformation can lead to the above mentioned gain changes, and most importantly how it enables STD at an inhibitory synapse to affect the operation performed by excitatory input.

chapter 6 **Determinants of gain modulation:** In this chapter we repeat the previous experiments under different conditions. We start by changing the STD level and calculate the gain to see if our results are robust to changes in STD. We then continue by calculating gain changes for different input condition, changing the synchronicity and regularity of the input and investigating their contribution to the STD effect.

chapter 7 Discussion: The last chapter of our thesis provides a general discussion of our findings, along with implications of our work and ideas for future research.

2

<div style="background:#9fd3f0;">

Gain modulation

</div>

2.1 Introduction

Neurons receive input from other neurons and output a sequence of action potentials, using a multitude of methods to encode information (Bialek et al., 1991; Softky, 1995; Oram et al., 1999; Rieke, 1999). One of these is the use of the action potential rate to encode their output, with a well-known example being the coding of sensory variables such as touch and pressure (Adrian and Zotterman, 1926). This rate-coding regime, which is likely to be used in the cortex (London et al., 2010), makes the relation between the output rate (F) and the input rate (f), known as the I–O function, a prominent feature in neural computation. This function, describing the response of the neuron, can be denoted as

$$\text{I–O} : f \rightarrow F \tag{2.1}$$

and describes how a neuron maps input rate onto output rate.

Neurons however, receive input from multiple sources, and one can distinguish between sources that drive the neuron, and sources that modulate it. Modulatory input can change the neuron's response, and thus its I–O function. These changes are not necessarily easy to describe, but two simple cases do stand out, and this is when modulatory input performs an additive or a multiplicative operation.

There are two distinct ways for these operations to be performed (Silver, 2010). To elucidate them, we must first define the I–O function as

$$F = R(f_d) \tag{2.2}$$

where the neuron's output rate (F) is given by the response of the neuron (R) as a function of the driving input (f_d). In the presence of a second, modulatory input (f_m), the resulting output rate will change. If this change is additive, then this addition can take place either in the input rate ($F = R(f_d + cf_m)$) or the output rate ($F = R(f_d) + cf_m$), where c is a scaling factor. In the same fashion, multiplicative operations are performed in either the input rate($F = R(f_d \times cf_m)$) or the output rate ($F = R(f_d) \times cf_m$). A summary of these changes in the I–O function can be found in Table 2.1.

$R_m(f_d, f_m)$	Input	Output
Additive	$R(f_d + cf_m)$	$R(f_d) + cf_m$
Multiplicative	$R(f_d \times cf_m)$	$R(f_d) \times cf_m$

Table 2.1: Linear modulations. Additive and multiplicative modulations applied in both the input and the output of the neuron. The equations show how the relation between the modulated response (R_m) of a neuron in the presence of a driving input (f_d) and a modulatory one (f_m), can be described as a function of the original response (R) . In all cases, c stands for a constant that can be defined experimentally.

These operations have different effects on a neuron's I–O function. Input additive and multiplicative operations result in a shift or a stretch of the x axis, respectively (Figure 2.1,a); while output additive and multiplicative operations shift and stretch the y axis (Figure 2.1,b).

Notice how, when an additive operation is performed, the I–O function will undergo a translation and so maintain its shape. On the other hand this is not the case for multiplicative operations. Regardless of whether the operation is performed in the input or the output of the neuron, a multiplicative operation will change the slope of the I–O curve (see section 2.4). This is known as gain modulation, and the modulatory input is known to perform gain control. Gain control is important for a number of reasons, ranging from changes of neuronal sensitivity to a specific input, to functional roles in brain processes. Some of the roles of gain modulation, along with a number of mechanisms underlying gain control, are discussed below.
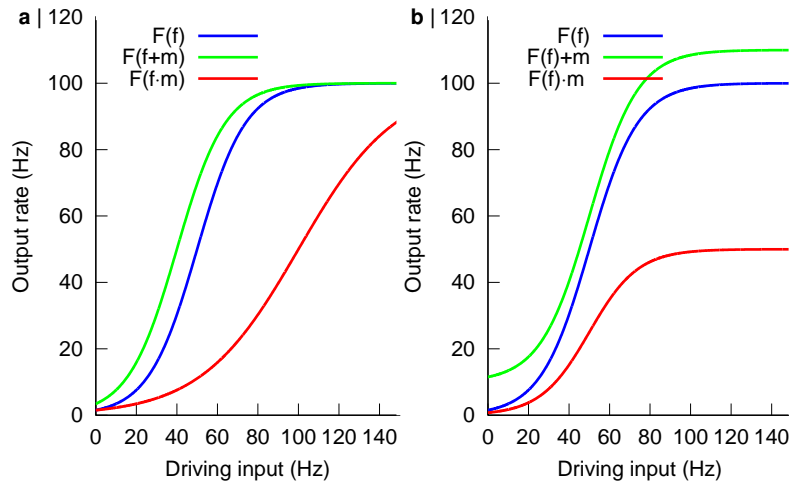
Figure 2.1: Example modulations. **a** | The I–O function of the neuron (blue), and after an additive (green) and multiplicative (red) operations performed in the input of the neuron. **b** | The same as a, with operations performed in the output of the neuron.

2.2   Roles of gain modulation

In the brain, multiplicative operations are widespread. From simple operations like scaling of the input-output relation that can improve information transmission (Brenner et al., 2000), to more complex ones, like the multiplicative scaling that orientation-tuning curves undergo during attention (McAdams and Maunsell, 1999), gain modulation is utilised in a wide range of brain functions (Salinas and Thier, 2000). It occurs in visual cortical neurons, where the gain of neurons that are direction-selective increases with attention (Treue and Martínez Trujillo, 1999), and during translation-invariant responses of some visual cortical cells (Tovee E. T. Azzopardi, P., 1994). It is also an intrinsic part of orientation tuning in cortical cells, allowing it to be contrast invariant (Anderson et al., 2000), while in inferior colliculus neurons neuronal gain is controlled by GABAergic inhibition (Ingham and McAlpine, 2005).

Since it is not possible to discuss all the roles of gain modulation in detail, we will focus on the posterior parietal cortex (PPC), where gain modulation was first discovered. There, gain modulation plays a key role in the encoding of spatial location (Mountcastle et al., 1981; Andersen and Mountcastle, 1983; Andersen et al., 1985), and in the coordinate transformation from

gaze to body coordinate system (Zipser and Andersen, 1988; Brotchie et al., 1995; Salinas and Abbott, 1995; Pouget and Sejnowski, 1997).

2.2.1   Coordinate transformation

Gain modulation was first observed in the encoding of spatial location, but was later found to play an important role in coordinate transformations. But what do we need coordinate transformations for? Assume that, while you stand still, you look at a glass of water. If you move your gaze to the left or the right, the position of the glass on the retina will change. Nonetheless, even if you do not look directly at it, you can always reach out and pick it up. This process requires a coordinate transformation, transforming the position of the glass from the retina coordinate system, to the body coordinate system.

The region of the brain receiving information about the position of the eyes and the head, and transforming it to body coordinates, is the posterior parietal cortex (PPC). To investigate the responses of the PPC neurons in the presence of a stimulus that moves in the head-centred coordinate system, but remains in the same position in the retina coordinate system, Mountcastle et al. (1981) trained macaque monkeys to fixate on a moving target light. By then displaying a visual stimulus in the same position relative to the moving target (that is, moving both stimuli at the same time), they were able to isolate the neuronal activity related to the position of the eye, from the one related to the position of the stimulus on the retina. The underlying behavioural state was defined as attentive fixation.

In another set of experiments, attentive fixation was used while providing visual stimuli, and the responses of parietal visual neurons had increased, compared to the responses during relaxed wakefulness, which corresponds to the state where the visual stimulus was not accompanied by the monkey fixating on a point. Light-sensitive neurons were also found to respond differently depending on the angle of the gaze, with the activity of an average neuron to tripling in response to a 20% shift in the optimal direction, an effect that was six times more likely to happen when the animal was receiving the stimuli while attentively fixating on a small target (Andersen and Mountcastle, 1983). This was consistent with the view that this area represents space in head-centred coordinates.

This view was reinforced by a following study, where Andersen et al.

(1985) investigated PPC neurons encoding the angle of a stimulus in the retina. The output rate of these neurons as a function of the stimulus position is given by a Gaussian function, with each neuron having a preferred direction at which it responds maximally (Figure 2.2); this is known as the response profile. Andersen and colleagues discovered a link between the response profile, and the angle of gaze. Not only did the respond profile change with the shift of the gaze angle, but it did so in a multiplicative manner. The activity of many neurons is thus subject to a gain factor that was a function of the eye position and the response profile of the retinal receptive field (Figure 2.2). This effectively means that the particular neurons are tuned for encoding information about the position of a stimuli in a head-centred coordinate frame.
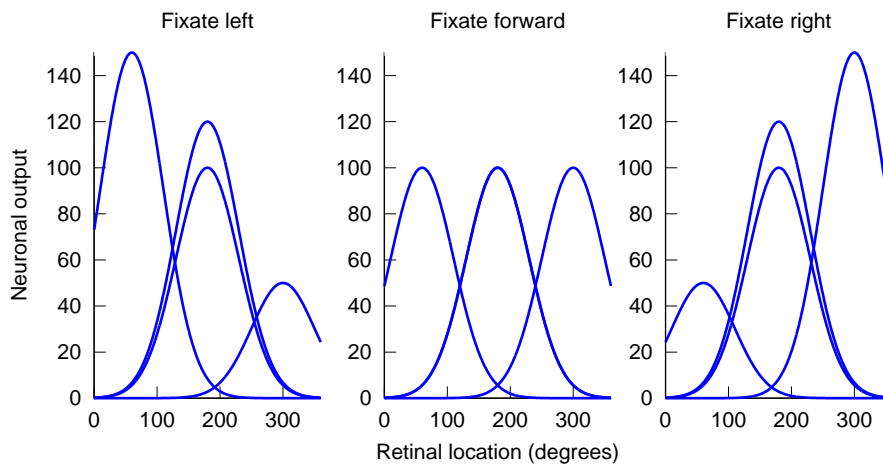
Figure 2.2: Idealised parietal neurons response. Idealised response of four parietal neurons to visual stimuli in a range of retinal coordinates, when the eyes are fixating in three different directions. The response of the neuron increases or decreases with the angle of gaze (Salinas and Thier, 2000).

To study the computational implications of gain modulation, Zipser and Andersen (1988) programmed a back-propagation neural network to simulate the responses of the subset of posterior parietal neurons, known to respond to both the location of the visual stimulus on the retina, and the position of the eye. They used a network of three layers that received the target's location on the retina, and the gaze angle as input, and, after training, could extract the eye-position-independent location. They then examined

the receptive fields of the middle layer, to find that they were gain modulated. This indicates that neurons with gain-modulated receptive fields, like the ones found in PPC neurons, can perform coordinate transformations.

2.3   Mechanisms of gain modulation

Gain modulation can be found in neurons in many brain areas, but not all of them use the same mechanism to change their gain. In fact there are a number of different processes responsible for gain control.

Shunting inhibition is one of the mechanisms responsible for multiplicative operations and gain changes. In the primary visual cortex, shunting inhibition accounts for the divisive gain modulation used in models to accurately predict particular visually driven responses (Carandini and Heeger, 1994), while in the electric fish it can regulate the gain of target neurons (Nelson, 1994). In vivo, neurons receive input from a great number of sources, and voltage is subject to stochastic noise. This synaptic noise lowers the input resistance of the neurons (Borg-Graham et al., 1998; Destexhe and Paré, 1999; Destexhe et al., 2003) , and is also crucial for gain operations. This is why some studies conducted with biologically realistic models that did not take into account synaptic noise only predicted shunting inhibition to have subtractive effects (Holt and Koch, 1997; Gabbiani et al., 1994; Capaday, 2002).

Noise due to synaptic input can enable voltage fluctuations, which enables the neuron to fire even in cases where the average voltage is below threshold. As a result, noise can affect the I–O function of a neuron (Mitchell and Silver, 2003; Anderson et al., 2000; Chance et al., 2002; Doiron et al., 2001; Tiesinga et al., 2000; Prescott and De Koninck, 2003; Higgs et al., 2006; Hansel and Van Vreeswijk, 2002; Miller and Troyer, 2002) even when input is sparse (Hô and Destexhe, 2000; Azouz, 2005; Shu et al., 2003).

Synaptic plasticity is also capable of affecting gain. In particular, gain can be affected by the short term increase or decrease of excitatory synaptic weights, that is short term synaptic facilitation or depression, respectively (Rothman et al., 2009). In effect, plasticity can change the way that neurons integrate input, which is usually linear (Cash and Yuste, 1998, 1999; Tamás et al., 2002; Gasparini and Magee, 2006; Holt and Koch, 1997), allowing multiplicative operations to be performed.

But the list of mechanisms responsible for gain control is long, so our intention is to discuss the ones related to noise and STD, and by no means provide a comprehensive list, something that has already by done by Silver (2010).

2.3.1 Synaptic noise

Information transmission between cells is noisy, mainly due to the intrinsic properties of synaptic input. When input from pre-synaptic neurons arrives at a synapse, a sequence of events leads to the increase and then decrease of the post-synaptic conductance for various ions (Figure 3.6). These conductance fluctuations, accompanied by stochastic noise in the synapses, can lead to voltage fluctuations in the post-synaptic response, that can lead to gain modulation.

The first gain control mechanism that we are going to discuss arises from background synaptic input. This mechanism was investigated by Chance et al. (2002), who explored changes in the response of a neuron as a result of background synaptic input. Using the dynamic clamp method, they were able to inject synaptic input into layer 5 pyramidal neurons, and to simulate excitatory and inhibitory input arriving from afferent neuron populations. They then injected constant current to drive the neuron, since they found this to produce effects similar to injecting excitatory synaptic input.

They found that increasing the level of background synaptic input could modulate neuronal gain, reducing the neuronal sensitivity to driving input. In particular, they studied the relation between input current and output rate (Figure 2.3). Separating the effects of the synaptic input variance, and the change in total conductance, they discovered that increasing the total conductance had an additive effect, shifting the I–O curve to the right (Figure 2.3,a); this result was consistent with previous studies (Holt and Koch, 1997). They also found that increasing the synaptic input variance had the opposite effect, shifting the corresponding curve to the left; this change was accompanied by a slope change that resulted in a tilt (Figure 2.3,b). Interestingly , when both noise and shunting inhibition were taken into account, the two additive shifts cancelled each other out, and the overall result was a tilt of the output rate as a function of input current (Figure 2.3,c). This cancelling of the two shifts accounts for the pure gain decrease introduced by the increase of background synaptic input; a gain control mechanism also
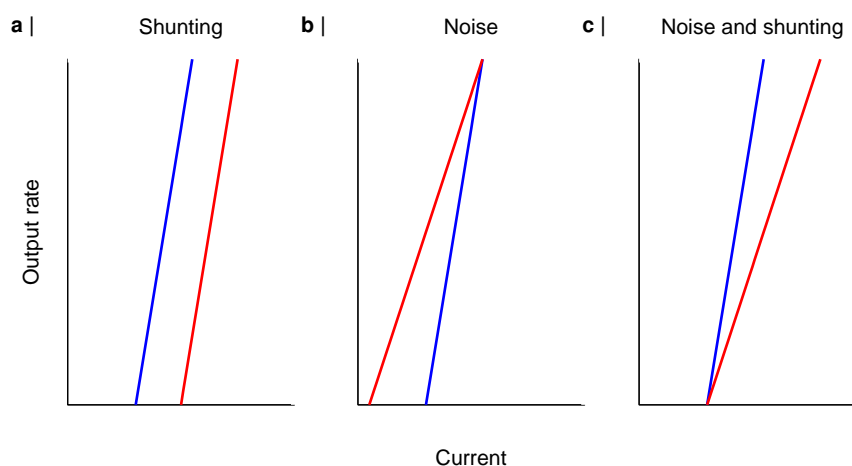
Figure 2.3: Modulation by shunting and noise. a | Idealised
response of a neuron without (blue) and with (red) shunting: shunt-
ing has an additive effect **b |** Idealised response without (blue) and
with (red) noise: noise has both a subtractive and divisive effect.
c | Original idealised response (blue) and modulated due to both
shunting and noise (red). Notice how the additive effect of shunting
and the subtractive effect of noise cancel each other out.

discussed by Priebe and Ferster (2002).

The effects of synaptic input on gain modulation have also been studied
in cerebellar granule cells. Using the dynamic clamp technique Mitchell and
Silver (2003) injected a tonic inhibitory conductance into granule cells while
driving them with a synaptic excitatory conductance; they then repeated
the experiment using a tonic excitatory conductance for the driving input.
They found tonic inhibition-mediated modulation to vary depending on the
nature of the driving input. When the neuron was driven by tonic excitat-
ory input, inhibition had a purely additive effect, shifting the I–O function
towards bigger values. However, for synaptic excitatory input, this shift was
accompanied by a gain change. To identify the effects of synaptic input, they
used both tonic and synaptic excitatory input to drive the neuron. Doing so,
they found that Poisson trains of synaptic inhibitory conductance performed
smaller shifts, and larger gain changes, compared to the ones performed by
tonic inhibitory input. They thus demonstrated how noise-mediated gain
modulation is not just influenced by noise in the excitatory input.

Moreover, in the neocortex, synaptic input was investigated, along with

dendritic saturation, and was found to play an important role in gain control by shunting inhibition. Using a biophysically realistic model of a layer V neocortical pyramidal neuron, Prescott and De Koninck (2003) examined the effects of synaptic shunting inhibition in the input, and found that shunting inhibition modulated firing rate in a divisive manner. In their study, they investigated the effects of shunting inhibition by removing the Hodgkin and Huxley models of ion channels from the soma and the proximal dendritic trees of the modelled neuron. In that way they were able to prevent spiking, and observe how shunting inhibition could affect the somatic voltage. They found shunting inhibition to reduce both the average somatic depolarization, and the fluctuation amplitude of the somatic voltage. By inducing voltage fluctuation to the soma with similar frequency and amplitude, thus considering the influence of noise in isolation, they found that noise alone could not account for the divisive effect of shunting inhibition. Without the effects of noise and dendritic saturation, shunting inhibition had a purely subtractive effect, and the addition of noise could only account for a modest gain change. Moreover dendritic saturation could not produce a big gain change either. It was thus the combination of noise and dendritic saturation that was necessary to account for gain control of the firing rate.

2.3.2 Gain modulation from synaptic depression

The input a neuron receives from afferent neuron depends on the strength of the synaptic connection. The notion that the strength of a synapse can change is very old (Hebb, 1949). Although originally this change was considered long-lasting or permanent, resulting when neurons fire together, other non-permanent changes are possible, with short term depression being one of them (Eccles et al., 1941). Short term depression can occur when the neurotransmitter vesicle supply decreases, due to previous stimulations, and the remaining pool of vesicles is not enough for the neuron to maintain the same response (Betz, 1970; Elmqvist and Quastel, 1965; Saviane and Silver, 2006). It can also occur due to desensitization of the post-synaptic receptors (Saviane and Silver, 2006; Trussell and Fischbach, 1989).

Short term depression has been shown to transform the arithmetic operations performed by cerebellar granule cells. Using dynamic clamp experiments, and neuronal simulations, Rothman et al. (2009) found that STD can enable a neuron to act as a multiplicative device. In particular, they showed

that, without STD when the neuron received an inhibitory input, the I–O curve would shift, indicating an additive operation. In the presence of STD, inhibitory input was found to have a second effect, changing the slope of the I–O function, and thus introducing a gain change. This was interesting because in effect, STD at the excitatory synapse was found to transform the operation performed by inhibition. To further investigate this gain change, they observed the mappings between input rate and average synaptic conductance, and between average synaptic conductance and output rate. They found that STD changed the relation between average conductance and input rate, while the relation between output rate and average conductance remained unaffected by STD. This was an indication that the observed gain changes took place due to the non-linearity introduced by STD in the input rate as a function of average conductance, a result that was not affected by synaptic noise.

To show that their results were not neuron specific, they repeated the simulation using a realistic, conductance based model of a layer 5 pyramidal neuron, receiving input from 400 excitatory and 30 inhibitory synapses. Again in the absence of STD, introduction of inhibition resulted in an additive shift, while in the presence of STD, this was accompanied by a gain change.

2.4   Determining arithmetic operations

There are various ways to determine arithmetic operations, mainly depending on the nature of the operation. If the additive or multiplicative operation is simple, it can be identified through visual inspection (Andersen et al., 1985; Brotchie et al., 1995; Abbott et al., 1997; Holt and Koch, 1997; Doiron et al., 2001; Mitchell and Silver, 2003; Prescott and De Koninck, 2003). A better practice is to use the reverse operation on the modulated curve, so that it will overlay with the original one. In an input additive operation this means shifting the curve (Steuber et al., 2011), and in an output multiplicative one, multiplying the output with a constant (Chance et al., 2002; Murphy and Miller, 2003; Ingham and McAlpine, 2005).

When the operation performed is non-linear, one of the ways to identify an operation is to perform curve fitting for the original and modulated data. Usually for this fitting, Hill like functions are used (Murphy and Miller,
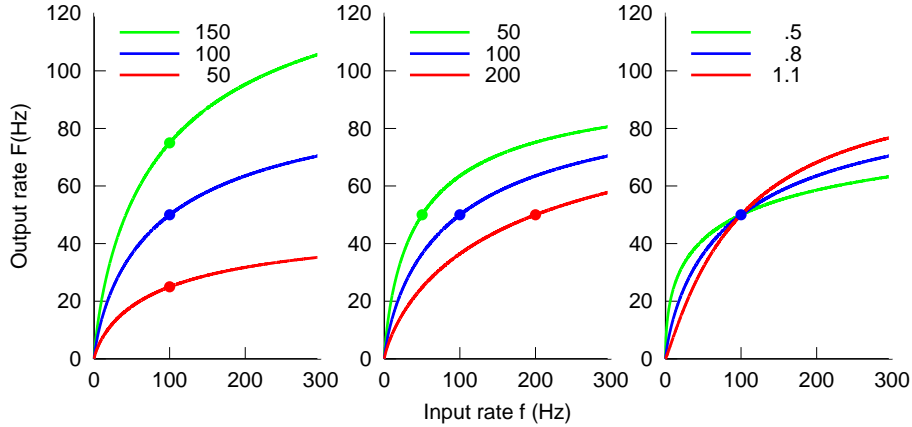
Figure 2.4: Hill function from Equation 2.3, using $F_{max} = 100$ $f_{50} = 100$ and $n = 0.8$, for various values of F_{max} (**left**), f_{50} (**centre**), and n (**right**).

2003; Rothman et al., 2009). Hill like functions are described by equations similar to (Silver, 2010)

$$F(f) = F_{MAX} \frac{f^n}{(f_{50})^n + f^n} \tag{2.3}$$

Where F is the output firing rate, and f the rate of the driving input. This function can take the shape of a sigmoid when n>1, and we can use it to identify the I–O curve by fitting F_{max}, f_{50}, and n. Various Hill functions with different F_{max}, f_{50}, and n can be seen in Figure 2.4.

Due to the intrinsic properties of this function, F_{max} and f_{50} correspond to the maximum output value, and the input rate that produces the half maximal response, respectively. After fitting the Hill function, we can then use a range of output frequencies to calculate the average gain. This range should account for the part of the curve with significant gain changes. For larger input rates, the I–O function saturates, and large changes in the input rate result in minor changes in the output rate. It is thus better not to include values near the beginning and end of the range. In previous work, the average gain, calculated using points corresponding to 5% and 75% of the maximum output rate was used (Rothman et al., 2009).

Since most of the I–O functions are monotonic, we can define the average gain of the functions as

$$F' = \frac{F_{75\%} - F_{5\%}}{f_{75\%} - f_{5\%}} \tag{2.4}$$

where $F_{75\%}$ and $F_{5\%}$ stand for 75% and the 5% of the maximum output value, and $f_{75\%}$ and $f_{5\%}$ are the input rates that correspond to these output values, respectively. We also follow previous studies (Rothman et al., 2009) and define the offset as the input rate corresponding to the half maximum output firing rate. That is

$$offset = f_{50\%} \tag{2.5}$$

Assuming that we have two I–O functions, and denoting with o the original one and with m the modulated one, we can find the percentage difference in gain using

$$\Delta Gain = \frac{F'_m - F'_o}{F'_o} \tag{2.6}$$

similarly for the change in offset

$$\Delta offset = offset_m - offset_o \tag{2.7}$$

However, regardless of the way used to identify an operation, one should always be careful since more than one operation can account for the same curve change. A good example is given by exponential functions (Silver, 2010), where

$$e^{f+m} = e^f \cdot e^m \tag{2.8}$$

which means that an input additive operation on the left, where m is added to input f, is equivalent to an output multiplicative operation on the right, where e^m is multiplied with the overall function. This is very common since for many modulated curves, there are two ways to go from a point on the original curve, to the corresponding point on the modulated curve. You can either go vertically or horizontally, thus assuming an output or an input operation, respectively.

Having multiple ways to describe the changes, it becomes important to justify why one operation is considered over the other. As we will see later for example, the operation performed by STD is classified as an input operation

since it changes neuronal input by depressing the synaptic conductance (section 5.4); and because this can account for how STD induces gain changes (section 5.5).

3

Computational neuroscience

The discovery of neurons in the brain dates back more than 100 years, with Santiago Ramón y Cajal being one of the first people able to actually see neurons and create detailed drawings of them (for review, see for example Sabbatini, 2003). One of these drawings, illustrating a section in the spinal cord, can be seen in Figure 3.1. However, these drawings did not reveal much about neuronal dynamics. A step towards understanding neuronal function came later when one of the pioneers, Donald Hebb, suggested that the strength of synapses could change due to activation (Hebb, 1949).

Our understanding of neuronal processes has changed dramatically since then. This leap in knowledge also involves computational models and mathematical theories of neuronal processes. Some of the best known theories, like the mathematical description of electrical membrane properties, have found their way into core neuroscience books (Kandel et al., 2000). Models with increased complexity, along with numerical methods, are usually discussed separately (Koch and Segev, 1998; Koch, 2004; Schutter, 2009; Sterratt et al., 2011), while at the same time related fields like artificial neural networks (Hertz, 1991) and spiking neural networks (Gerstner and Kistler, 2002) have emerged.

To simulate a neuron using a biologically realistic model requires the combination of many theories, such as linear-cable theory Rall (1962), and the Hodgkin-Huxley model (Hodgkin and Huxley, 1952). This is because neurons are cells, with numerous proteins playing various roles in input processing. A detailed model found in an online database (Migliore et al., 2003) can incorporate a number of theories and models, along with a set
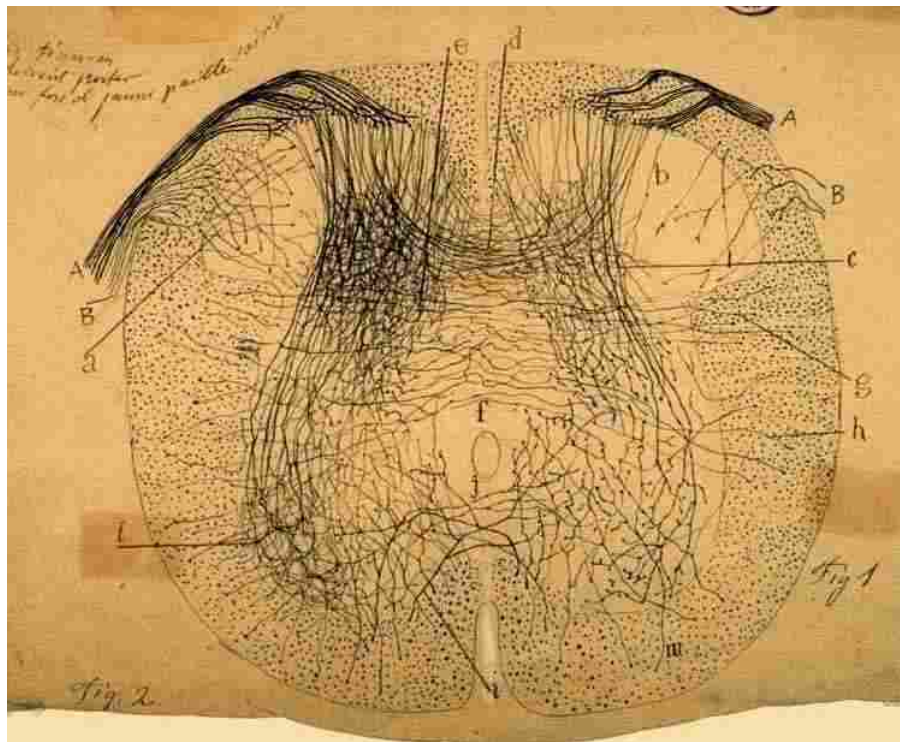
Figure 3.1: Example of one of Cajal's drawings. Drawing of
a spinal cord section (Sabbatini, 2003).

of variables. From the membrane's electrical activity and the cable equa-
tion, to compartmental modelling, and from the Hodgkin-Huxley model to
various models of ion channels, detailed neuronal models hold the accumu-
lated knowledge related to a specific neuron. Although it is not necessary
for someone to know all of these theories, since modern simulators such as
NEURON (Carnevale T. and Hines L., 2006) and GENESIS (Bower and
Beeman, 2014) implement them automatically, it is still a good idea to have
a good grasp of them.

It is not possible to discuss all methods and theories here, but we should
discuss at least three of them. Firstly, we are going to discuss the cable
theory, a mathematical description of ion movement inside a passive cell.
Then, and to move towards active neurons, we will discuss the way neurons
communicate through action potentials, and the Hodgkin-Huxley model.
Last but not least, we are going to introduce simple synaptic models, and
explain how they can be altered to incorporate short term depression.
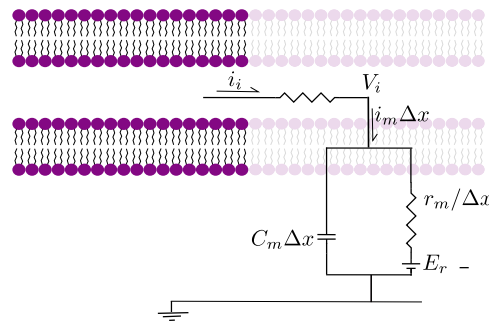
Figure 3.2: The equivalent circuit of the neuronal membrane. The membrane consists of a capacitance, a conductance and an electromotive force. For the derivation of the cable theory we use values per, or times, unit length or area, for example capacitance per unit length and area. This means that the solution applies to a continuous rather than a discrete circuit.

3.1 Cable theory

Ions moving in the internal and the external mediums of the cell create electrical currents that underlie information processing in the brain. To simulate these current flows we can describe the cell membrane as an electrical circuit (Figure 3.2). In case of the passive cable this circuit can be described using simple electrical components such as capacitors, resistors and batteries. The main difference to the widely known electrical circuits is that in the cell, ions, and not electrons, are the carriers of electrical charges. In nature cables are not passive and ion channels, ion pumps and other structures add to the complexity, but this will not be discussed here.

Our goal is to derive an equation that describes the deviation of the intracellular voltage from its resting value with respect to time t, and position along the cylinder x. The definition of this deviation can be seen below

$$V = V_i - V_e - E_r \tag{3.1}$$

Where E_r denotes the passive reversal potential that constitutes the resting membrane voltage and V_i and V_e the potential in the intracellular and extracellular areas, respectively. We assume that membrane properties, like capacitance, conductance and reversal potential, remain uniform. To do so we assume that the core conductor is cylindrical and uniform.

We know from Ohm's law that we can find the voltage difference along

a conductor by using

$$V = I \cdot R \tag{3.2}$$

We define r_i in $[\Omega/cm]$ to be the intracellular resistivity per unit length along the cable, and i_i in $[A]$ the intracellular current, taken positive when flowing to the right. Applying Ohm's law to find V between two points we have $V = -i_i r_i \Delta x \Leftrightarrow V/\Delta x = -i_i r_i$. Taking the limit of Δx approaching zero we find

$$\frac{\partial V}{\partial x} = -i_i r_i \tag{3.3}$$

Having assumed uniform properties, r_i remains constant, and differentiating the above equation with respect to x will thus result in

$$\frac{\partial^2 V_i}{\partial x^2} = -r_i \frac{\partial i_i}{\partial x} \tag{3.4}$$

Notice the term di_i/dx that emerged through the derivation. This term is by definition the rate of change for the intracellular current per unit length. Since the amount of current leaving the intracellular area per dx is the same as the one passing through the membrane per dx, these two must be equivalent. Taking into consideration that a rise in the former will result in a fall of the latter we can define the membrane current density per unit length (i_m) as

$$i_m \equiv -\frac{\partial i_i}{\partial x} \tag{3.5}$$

Notice the difference between i_i and i_m. The first is the intracellular current along the cable in $[A]$, while the second is the membrane current density per unit length in $[A/cm]$. Combining Equation 3.4, and Equation 3.5 we have

$$\frac{\partial^2 V_i}{\partial x^2} = r_i i_m \tag{3.6}$$

Differentiating Equation 3.1 for constant E_r, and making the further assumption that the extracellular potential V_e also remains stable we have $\partial^2 V/\partial x^2 = \partial^2 V_i/\partial x^2$. This means that in Equation 3.6 we can substitute V_i for V. Doing so, and multiplying by r_m/r_i we have

$$\frac{r_m}{r_i}\frac{\partial^2 V}{\partial x^2} = r_m i_m \tag{3.7}$$

Now it is time to move to the membrane. We will first have to define some quantities of interest. For the capacitance we have the membrane capacitance per unit area C_m in $[F/cm^2]$ and the membrane capacitance per unit length $c_m = C_m \pi d$ in $[F/cm]$, where d is the diameter of the cylinder. For the conductance of the membrane we have the membrane conductance per unit area G_m in $[S/cm^2]$ and per unit length $g_m = G_m \pi d$ in $[S/cm]$. Knowing the conductance we can also find the resistance times unit area $R_m = 1/G_m$ in $[\Omega cm^2]$ and times unit length $r_m = 1/g_m$ in $[\Omega cm]$. Having defined all of the above we can describe the membrane current density per unit length as

$$i_m = c_m(\partial V/\partial t) + (V_i - V_e - E_r)/r_m \tag{3.8}$$

Substituting using the definition of V in Equation 3.1, and then multiplying by r_m we have

$$i_m r_m = \tau_m(\partial V/\partial t) + V \tag{3.9}$$

where τ_m represents the passive membrane time constant and equals

$$\tau_m = r_m c_m = R_m C_m \tag{3.10}$$

Finally we can combine Equation 3.7 and Equation 3.9 and set $\lambda = \sqrt{r_m/r_i}$ to reach

$$\lambda^2 \frac{\partial^2 V}{\partial x^2} = V + \tau_m \frac{\partial V}{\partial t} \tag{3.11}$$

The above is known as the Cable Equation and was derived using only the dimension along the cable. To derive it we also assumed the neuron to be a cylindrical core conductor, uniform with extracellular isopotentiality.

The cable equation can be solved analytically for various boundary conditions, but is usually solved numerically as part of neuron simulations. Although it describes voltage changes in neurons, it is limited to passive neurons. This does not mean that when active mechanisms are taken into account, the cable equation is rendered unusable. Rather, active mechanisms must be modelled in addition to cable theory. One of the best known

examples of active mechanisms underlies the generation of the action potentials, and was first inferred by Alan Hodgkin and Andrew Huxley (Hodgkin and Huxley, 1952).

3.2   Hodgkin–Huxley model

The most common method for neurons to convey information is by means of action potentials. In effect, action potentials are a quick rise of the membrane potential (depolarization), followed by a sharp fall (repolarization), that propagate along the neuron's axon. The first quantitative description of the action potential was given by Hodgkin and Huxley (1952).
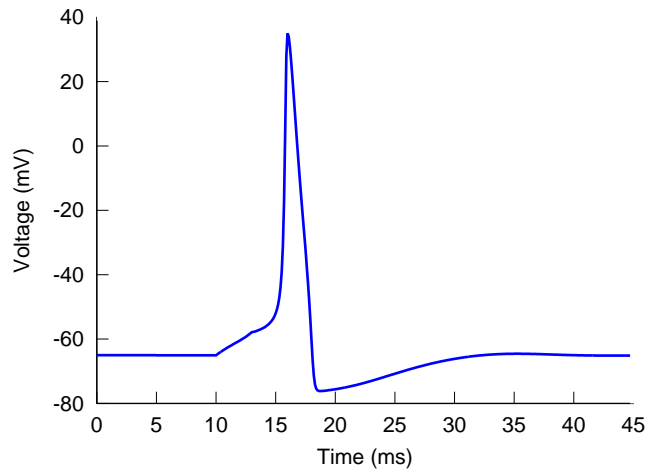
Figure 3.3: Action potential. Neurons receive excitatory input capable of increasing their membrane potential. Action potentials are generated when the membrane potential reaches a certain value, here −55 V, which is known as threshold.

In their work, they described the ion current mechanism underlying voltage fluctuations and the creation of the action potential. Here, we will not consider the experimental nature of Hodgkin and Huxley's work. Instead we focus on the quantitative description of the proposed mechanisms. At the same time, we combine most of the equations introduced in this section and solve them numerically using the variable step solver lsode in GNU octave to simulate an action potential. The values of interest are then plotted in Figure 3.3 Figure 3.4 and Figure 3.5.

We consider the neuron membrane to be an electrical circuit. This circuit

is responsible for the flow of currents from the extracellular to the intracellular space and vice versa. This circuit incorporates the ion movement in the form of a membrane capacitor per unit area (C_m) and three ion currents: the sodium (I_{Na}) potassium (I_K) and leakage (I_L) current. The total current that passes through the membrane then changes the membrane voltage based on Kirchhoff's Law

$$C_m \frac{dV}{dt} = -I_{Na} - I_K - I_L \tag{3.12}$$

To gain an insight into these currents Hodgkin and Huxley applied a voltage clamp, thus setting the membrane potential to a constant value. Having constant voltage imposes a zero net current by setting the left term of Equation 3.12 to zero. That is

$$0 = -I_{Na} - I_K - I_L$$

For every ion, there is a specific membrane potential, also known as reversal potential, for which the average current flowing through the membrane is zero. The deviation of the membrane potential from this value will lead to an ion current, and is thus known as driving force. The exact value of the flowing current is then the product of the membrane conductance for that ion, and the driving force. Thus, we have

$$I_{Na} = g_{Na}(V - E_{Na}) \tag{3.13}$$
$$I_K = g_K(V - E_K) \tag{3.14}$$
$$I_L = \bar{g}_L(V - E_L) \tag{3.15}$$

where g_{Na}, g_K and $\bar{g}_L$ stand for the sodium, potassium, and leak conductance, respectively. Similarly E_{Na}, E_K and E_L, denote the corresponding reversal potentials. As we will see in the next section, the values of g_{Na} and g_K vary with time and voltage; in contrast the bar in $\bar{g}_L$ denotes a constant value.

3.2.1 Potassium current and ion channels

Using a voltage clamp Hodgkin and Huxley were able to keep the membrane potential at a desired value. By then changing the extracellular ion

concentration they were able to identify which ions contribute the most. By replacing sodium ions with an organic cation, they could record I_K and calculate g_K using Equation 3.14. The resulting time course of the potassium conductance during a depolarising voltage step is shown in Figure 3.4.
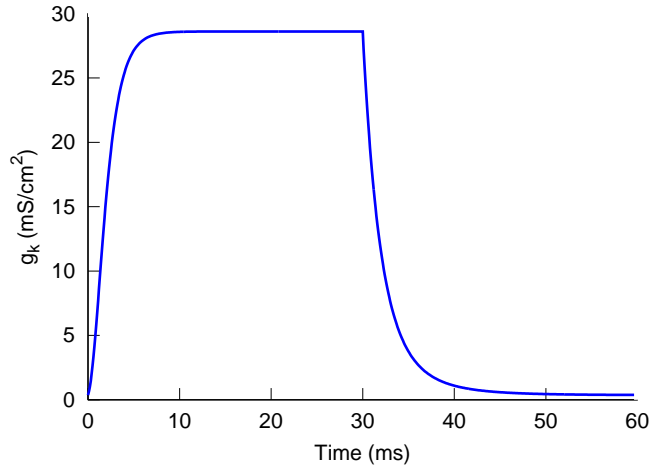
Figure 3.4: Potassium conductance. Time course of the potassium conductance during a depolarising voltage step. The depolarization results in an increase of the potassium conductance, followed by a decrease to zero when the cell returns to the membrane resting potential.

To explain these results, they introduced the concept of ion channels, controlled by gating particles. Each of these gates can be in an open or a closed state. This can be encapsulated in the following kinetic scheme

$$C \underset{\beta_n}{\overset{\alpha_n}{\rightleftharpoons}} O$$
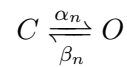
This kinetic scheme states that the gates of the ion channels can move, from an open state (O), to a closed state (C). The rate coefficients α_n and β_n control the speed of these transitions. If n denotes the fraction of gates in the open state, then the fraction of gates in the closed state will be $1 - n$. At time t, $\alpha_n(1 - n)$ gating particles will enter the open state, while $-\beta_n n$ gates will move to the closed state. Overall we can describe this process with a differential equation

$$\frac{dn}{dt} = \alpha_n(1 - n) - \beta_n n \tag{3.16}$$

the general solution of the above can be found as

$$\frac{dn}{dt} + (\alpha_n + \beta_n)n = \alpha_n$$

$$e^{(\alpha_n+\beta_n)t}(\frac{dn}{dt} + (\alpha_n + \beta_n)n) = e^{(\alpha_n+\beta_n)t}\alpha_n$$

and then integrating for t

$$e^{(\alpha_n+\beta_n)t}n = \frac{\alpha_n}{\alpha_n + \beta_n}e^{(\alpha_n+\beta_n)t} + C$$

$$n(t) = \frac{\alpha_n}{\alpha_n + \beta_n} + Ce^{-(\alpha_n+\beta_n)t}$$

and by setting $n_\infty \equiv n(\infty) = \alpha_n/(\alpha_n + \beta_n)$ and $n_0 \equiv n(0)$ we can extract $C = n_0 - n_\infty$. Finally we define the time constant to be $\tau_n = 1/(\alpha_n + \beta_n)$ so that

$$n(t) = n_\infty + (n_0 - n_\infty)e^{-t/\tau_n} \qquad (3.17)$$

Trying to find the α and β values, Hodgkin and Huxley found that both of them are a function of voltage. This does not change the above equation since it was derived using a voltage clamp, and the values of n_0, n_∞ and τ_n remain constant for a particular voltage. They then moved on to collecting measurements of the conductance and extracting the α and β values for different voltages. In this way they found continuous equations able to fit the experimental data. These were

$$\alpha_n = 0.01\frac{V + 55}{1 - e^{(-(V+55)/10)}} \qquad (3.18)$$

$$\beta_n = 0.125e^{-(V+65)/80} \qquad (3.19)$$

Knowing the activation variable n, finding the actual conductance is just a matter of multiplication with the maximum conductance. The maximum conductance ($\bar{g}_K$) is constant. However, what is interesting is their use of n^4 to describe the potassium conductance, assuming that the channel is gated by four particles, which happens to correspond to the four subunits of the delayed rectifier potassium channel. The resulting equation that describes

the current is

$$I_K = \bar{g}_K n^4 (V - E_K) \tag{3.20}$$

Considering all of the above, one needs four equations to describe the potassium dynamics: Equation 3.16, Equation 3.18, Equation 3.19, and Equation 3.20.

3.2.2   Sodium current and leak current

The other active current studied was the sodium current (I_{Na}). Sodium behaves differently than potassium since it is inactivated, meaning that after a period of staying open, the channel will close and stay inactive for a certain time. During an action potential this translates in a sharp increase of the average conductance followed by a steep decrease as we can see in Figure 3.5. Even though the depolarization persists throughout time, g_{Na} reaches a maximum value and then decreases to zero.
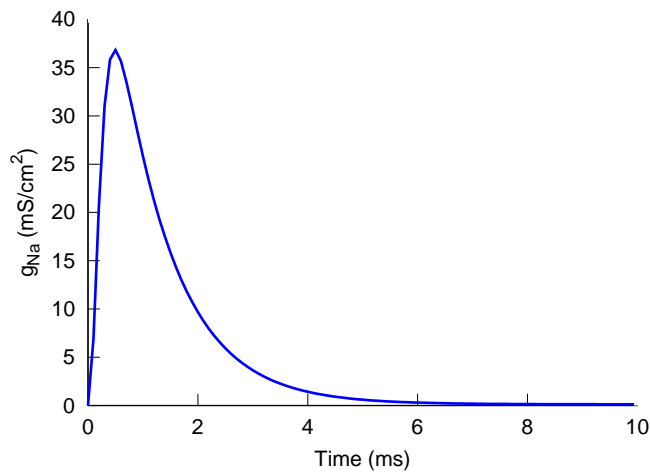
Figure 3.5: Sodium conductance. The sodium conductance as a function of time during a depolarising voltage step. We can see that the channel inactivates after a while and the conductance returns to zero, even though the depolarization is maintained throughout the plotted time.

This can be explained by the existence of two gating particles, instead of one. Only in this case, one particle results in the activation (m) and the other in the inactivation (h) of the channel. Using a similar analysis as before, and fitting their data, Hodgkin and Huxley came up with the

equations below to describe the sodium current.

$$I_{Na} = \bar{g}_{Na} m^3 h (V - E_{Na}) \tag{3.21}$$

$$\frac{dm}{dt} = \alpha_m(1 - m) - \beta_m m \quad \frac{dh}{dt} = \alpha_h(1 - h) - \beta_h h \tag{3.22}$$

$$\alpha_m = 0.1 \frac{V + 40}{1 - \exp(-(V + 40)/10)} \quad \alpha_h = 0.06 \exp(-(V + 65)/60) \tag{3.23}$$

$$\beta_m = 4 \exp(-(V + 65)/18) \quad \beta_h = \frac{1}{\exp(-(V + 35)/10) + 1} \tag{3.24}$$

Finally there is the leak current that consists of all the other ions. The leak current can be found using

$$I_L = \bar{g}_L (V - E_L) \tag{3.25}$$

Having identified the sodium (Equation 3.21), potassium (Equation 3.20), and leak (Equation 3.25) currents, we can substitute them in the membrane equation (Equation 3.12) to find how the potential across the membrane changes over time. Doing so we have

$$C_m \frac{dV}{dt} = -\bar{g}_L(V - E_L) - \bar{g}_{Na} m^3 h (V - E_{Na}) - \bar{g}_K n^4 (V - E_K) \tag{3.26}$$

However, this equation alone is not sufficient to describe all changes in a neuron. This is because neurons vary in size and shape, with dendrites forming both simple and complex trees. This means that their modelling can not be simplified to a simple cable. To get a realistic representation of a neuron, one should create a model that takes into account the neuron's morphology. A method to do so was first introduced by Rall (1964), who divided the dendritic structure into smaller parts, in a way that the morphology of a part resembles that of a cable, but ensuring that it is small enough to be considered isopotential. Today, this method of compartmental modelling is the de facto method for simulating electrophysiologically complex realistic neurons.

3.3   Synaptic models

To distribute information, the nervous system must have an efficient way for neurons to communicate. Evolution has provided them with a wide variety of synaptic mechanisms, both electrical and chemical, but modelling their behaviour can be challenging. Although there are a wide variety of models, both phenomenological and functional, to introduce synaptic modelling we will consider a simple model of a chemical synapse.

3.3.1   Chemical synapses: Difference of two exponentials

When an action potential (AP), travelling along the axon of the pre-synaptic neuron, arrives at a chemical synapse, it results in the release of neurotransmitter vesicles, and thus the diffusion of neurotransmitters across the synaptic cleft. Neurotransmitters then bind to receptors on the post-synaptic cell, and induce a current, know as post-synaptic current (PSC) (Kandel et al., 2000). Depending on the synapse this current can depolarise the neuron, and thus called excitatory post-synaptic current (EPSC), or hyperpolarise it, and called inhibitory post-synaptic current (IPSC). The current inducted by a single pre-synaptic AP at time t_s, can be described by

$$I_{syn}(t) = g_{syn}(t)\left(V(t) - E_{syn}\right) \tag{3.27}$$

Where E_{syn} is the synapse's reversal potential, $V(t)$ the voltage across the membrane, and $g_{syn}(t)$ the post-synaptic conductance with regards to time. The post-synaptic conductance can also be distinguished as g_{exc} and g_{inh} for an excitatory and an inhibitory synapse, respectively. This change of conductance, that follows the arrival of a pre-synaptic AP constitutes the effect of the neurotransmitters binding, and it can be phenomenologically described by a difference of two exponentials (Figure 3.6,a). That is

$$g_{syn}(t) = \bar{g}_{syn}\frac{\tau_1\tau_2}{\tau_1 - \tau_2}\left(\exp(-\frac{t - t_s}{\tau_1}) - \exp(-\frac{t - t_s}{\tau_2})\right) \tag{3.28}$$

Where $\bar{g}_{syn}$ is the maximum conductance, t_s denotes the AP's arrival time, and τ_1 and τ_2 are the decay and rise time constants, respectively. Finally, the term $\tau_1\tau_2/(\tau_1 - \tau_2)$ is a normalisation factor.

However, knowing the response of a post-synaptic cell to a single AP is
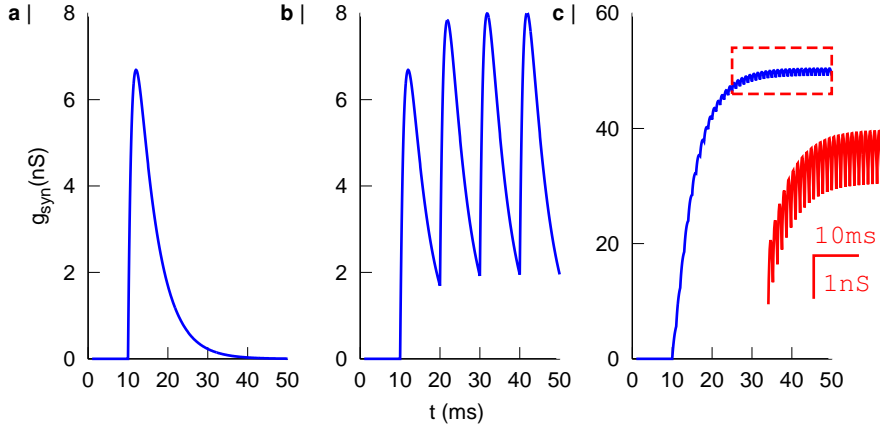
Figure 3.6: Post synaptic conductance. **a** | Conductance
response to an AP that arrives at $t = 10$ ms, described by a double
exponential synapse (Equation 3.28) with $\bar{g}_{syn} = 10$ nS, $\tau_1 = 5$ ms
and $\tau_2 = 1$ ms **b** | The same for a train of action potentials starting
at $t = 10$ ms, with APs arriving every 10 ms. This time the time
course of the conductance is given by Equation 3.29. **c** | A similar
train as **b**, with the interval between APs dropped to 1 ms. In red,
re-plot of the conductance inside the box, on the same scale as **a** and
b. Notice how the increase of the input rate results in a decrease in
conductance fluctuations.

not sufficient, since neurons usually receive input from trains of APs. Often,
the response of a synapse remains unaffected by preceding input, and we
can thus find the overall response by summing the responses to individual
incidents. Due to this superposition property, the conductance as a function
of time (t) as a response to APs arriving at time t_s ($t > t_s$) will be

$$g_{syn}(t) = \sum_{i=1}^{n} \bar{g}_{syn} \frac{\tau_1 \tau_2}{\tau_1 - \tau_2} \left(\exp(-\frac{t - t_s^i}{\tau_1}) - \exp(-\frac{t - t_s^i}{\tau_2}) \right) \qquad (3.29)$$

The response of an excitatory post-synaptic conductance, with $\bar{g}_{syn} = 10$ ns,
$\tau_1 = 5$ ms and $\tau_2 = 1$ ms, for one, a few, and many APs can be found in
Figure 3.6.

It is worth mentioning that an increase of input rate, results in a decrease
of conductance fluctuations. This can prove to be important since for high
input frequencies, conductance fluctuations are small, eliminating effects

related to the shape of single PSC, resulting in a response similar to a step function, which is equivalent to tonic input. That means that for high frequencies effects related to large voltage fluctuations might disappear.

3.3.2   Relationship between input rate and average conductance.

The average conductance of a synapse (G_{syn}) that results from a train of APs can be calculated analytically. Assuming that the strength of the synapse remains constant, and that there is no variability in the inter-spike intervals (ISI) we can investigate how different input frequencies f_c can lead to different average conductances $(G_{syn}(f_c))$, where the subscript c stands for constant and denotes the lack of variability; this is to avoid confusion with the average input frequency f, that will be used later on. Although we are not going to use the end result of the calculation directly, it is useful since it can give us an insight into this relationship.

As we saw in the previous section, the equation that describes the conductance of the synapse after the arrival of an AP is:

$$g_{syn}(t) = \bar{g}_{syn} \frac{\tau_1 \tau_2}{\tau_1 - \tau_2} \left(\exp\left(-\frac{t - t_s}{\tau_1} \right) - \exp\left(-\frac{t - t_s}{\tau_2} \right) \right)$$

To find G_{syn} we must first calculate the integral of $g_{syn}(t)$. To do so we integrate starting from the arrival of the AP (t_s) to infinity.

$$
\begin{aligned}
\int_{t_s}^{\infty} g_{syn}(t)dt &= \bar{g}_{syn} \frac{\tau_1 \tau_2}{\tau_1 - \tau_2} \left(\int_{t_s}^{\infty} \exp\left(-\frac{t - t_s}{\tau_1} \right) dt - \int_{t_s}^{\infty} \exp\left(-\frac{t - t_s}{\tau_2} \right) dt \right) \\
&= \bar{g}_{syn} \frac{\tau_1 \tau_2}{\tau_1 - \tau_2} \left(-\tau_1 \exp\left(-\frac{t - t_s}{\tau_1} \right) \Big|_{t_s}^{\infty} + \tau_2 \exp\left(-\frac{t - t_s}{\tau_2} \right) \Big|_{t_s}^{\infty} \right) \\
&= \bar{g}_{syn} \frac{\tau_1 \tau_2}{\tau_1 - \tau_2} (\tau_1 - \tau_2) \\
&= \bar{g}_{syn} \tau_1 \tau_2 \tag{3.30}
\end{aligned}
$$

The result of this calculation, leads to a constant that depends on the time constants of the synapse, and the maximum synaptic conductance $\bar{g}_{syn}$. Since the conductances are superimposed, to calculate the average conductance for a train of APs that arrive with a frequency f_c, we have to sum the

previous result for all APs, and divide by time.

$$G_{syn}(t) = \left(\sum_{n=1}^{n} \int_{t_s}^{\infty} g_{syn}(t)dt \right) / t$$

where n, is the number of action potentials arrived until t, given by $n = f_c \cdot t$. Substituting, we have

$$G_{syn}(f_c) = \bar{g}\tau_1\tau_2 f_c \tag{3.31}$$

This linear relationship between input frequency and average conductance will be used in later chapters.

3.4 STD and synaptic transmission

Neurons can communicate by using trains of APs. As we saw previously, the reaction of a neuron to multiple presynaptic APs is often assumed to be a linear summation of the independent effects. However, this is not always the case, as the arrival of an AP might alter post-synaptic effects of subsequent APs (Figure 3.7,a). This change can be a depression or a facilitation, decreasing or enhancing following responses, respectively (Dittman et al., 2000). Time moderates these effects, and depending on how long it takes for the neuron to reach its initial state and again be able to respond fully, we can distinguish between short-term and long-term depression, and short-term and long-term facilitation. Short term depression is known, among other mechanisms, to account for a number of temporal characteristics of cortical neurons (Chance et al., 1998), while short-term synaptic facilitation has been theorised to account for the maintenance of working memories (Mongillo et al., 2008). Here we are interested in computational models of depression that has short term affects. For this we will consider two models, both of them involving the use of a depression factor applied to g_{syn}.

3.4.1 Dynamic variables STD model

The first model we discuss was developed in order to describe STD at excitatory synapses of the primary visual cortex (Varela et al., 1997). The main idea in this model is that the conductance amplitude (A) is a product of an initial amplitude (A_0) and a number of depression (D) and facilitation

(Fac) factors. That is

$$A = A_0 Fac \cdot D_1 D_2 D_3 \tag{3.32}$$

with different time constants and scaling factors used for every depression and facilitation factor. However one does not have to include all the complexity in this model. Simpler variants of this model, omitting the facilitation factor and using only one depression factor; or using only the facilitation factor, can also be used.

When the pre-synaptic AP arrives, the various depression factors (D) are multiplied with a scaling factor δ ($D \rightarrow \delta D$), while between stimuli they recover exponentially following the rule:

$$\tau_D \frac{dD}{dt} = 1 - D$$

where τ_D is a time constant. Consequently in-between synaptic inputs the depression factor is described by

$$\tau_D \frac{dD}{dt} = 1 - D \Leftrightarrow$$
$$\int \frac{dD}{1 - D} = \int \frac{dt}{\tau_D} \Leftrightarrow$$
$$-log(1 - D) + C = \frac{t}{\tau_D} \Leftrightarrow$$
$$D = 1 - (1 - D_0)e^{-t/\tau_D} \tag{3.33}$$

where D_0 stands for the depression factor after the arrival of the last synaptic input. Since D depresses the conductance amplitude, we can assume that it will have the same effect on the average conductance. We can thus combine Equation 3.31 and Equation 3.33 to find

$$G_{syn}(f_c) = g\tau_1\tau_2 f_c \cdot (1 - \overline{(1 - D_0)}e^{-t/\tau_D}) \tag{3.34}$$

When the input rate is constant, D reaches an equilibrium, and the increase during inter-spike intervals equals the decrease due to the multiplication with a scaling factor. The effects of this model on the average synaptic conductance for an IaF neuron can be seen in Figure 3.7,b.
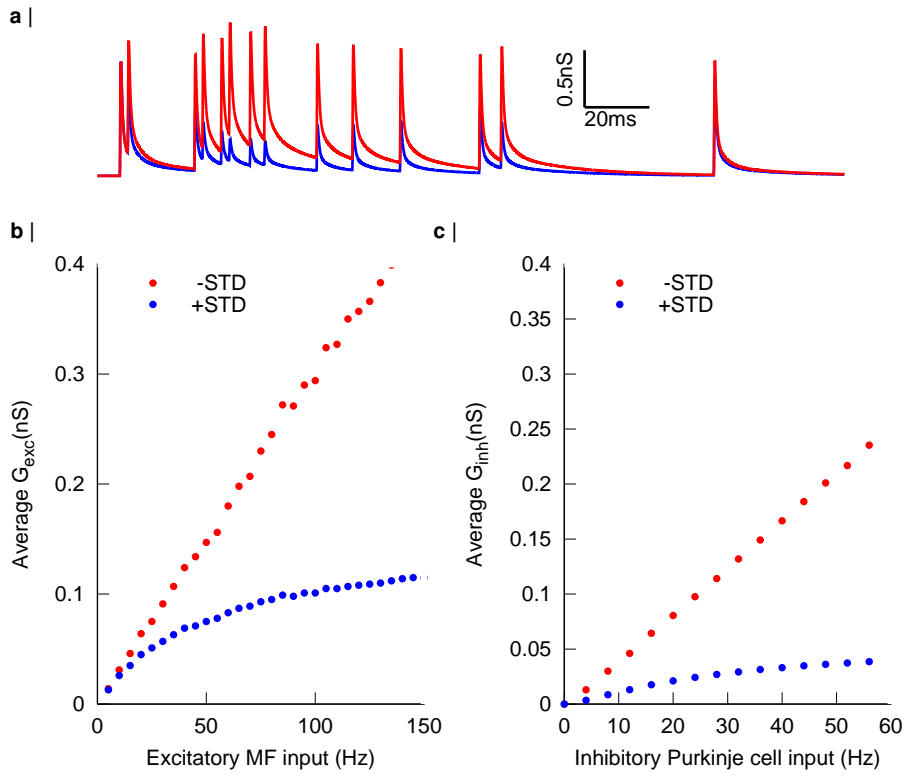
Figure 3.7: Effects of STD on synaptic conductance. a |
Conductance trace in the absence (red) and presence (blue) of STD
for 60Hz of input rate. STD was based on the Varela et al. (1997)
model, using $\delta = 0.5$. **b |** Average excitatory conductance G_{exc} for
a single MF as a function of input rate f in the absence (red) and
presence (blue) of STD based on the Varela et al. (1997) model.
Simulation data correspond to the IaF model used in chapter 4.
c | Same as in **b** for the average inhibitory conductance calculated
over all PC synapses, and the STD model corresponding to Shin
et al. (2007). This time simulation data correspond to a biologically
realistic model of a CN neuron, as found in chapter 5.

3.4.2   Pre-synaptic release probability STD model

Another synapse that exhibits STD is the GABAergic synapse between PCs and CN neurons. This synapse was investigated experimentally by Pedroarena and Schwarz (2003), and a computational model based on their findings was derived later (Shin et al., 2007). This model assumes that the underlying mechanism of STD are changes in the pre-synaptic vesicle release probability (R). The steady state level of the pre-synaptic release probability (R_{ss}), and the depressions time constant (τ) are given by

$$R_{ss}(f_{inst}) = 0.08 + 0.6e^{-2.84f_{inst}} + 0.32e^{-0.02f_{inst}} \qquad (3.35)$$

$$\tau(f_{inst}) = 2 + 2500e^{-0.274f_{inst}} + 100e^{-0.022f_{inst}} \qquad (3.36)$$

where f_{inst} corresponds to the instantaneous firing rate and is found by inverting the last ISI. Both R_{ss} and τ are updated on the arrival of then n^{th} AP, and we can then use the new values to calculate R.

$$R_n = R_{n-1} + (R_{ss} - R_{n-1})\left(1 - e^{-\frac{ISI_n}{\tau}}\right) \qquad (3.37)$$

with R_{n-1} and ISI_n denoting the release probability and the inter-spike interval for the $(n-1)^{th}$ and n^{th} action potential, respectively. We can then calculate $G_{syn}(t)$ using

$$G_{syn}(t) = G_{pre} + A\frac{G_{max}}{\tau_1 - \tau_2}R_n(e^{-t/\tau_1} - e^{-t/\tau_2}) \qquad (3.38)$$

where G_{pre} is the synaptic conductance as a result of previous APs, and the term that follows is the contribution of the current AP, with A, τ_1 and τ_2 as constants.

To get an insight into the relationship between the input frequency and the average conductance, we can work as previously and assume a constant input frequency with no variability between ISIs (f_c). After some time, this will result in a constant R, and thus $R_{n-1} = R_n$. Substituting into Equation 3.37 we have

$$\begin{aligned} R_n =& R_n + (R_{ss} - R_n)\left(1 - e^{-\frac{ISI_n}{\tau}}\right) \Leftrightarrow \\ 0 =& (R_{ss} - R_n)\left(1 - e^{-\frac{ISI_n}{\tau}}\right) \end{aligned}$$

and because $ISI_n/\tau \neq 0$ we have $R_n = R_{ss}(f_c)$ and

$$R_n(f_c) = 0.08 + 0.6e^{-2.84f_c} + 0.32e^{-0.02f_c} \tag{3.39}$$

Having calculated the depression factor, we can substitute into Equation 3.31 to find

$$G_{syn}(f_c) = R_n(f_c)AG_{max}\tau_1\tau_2 f_c \tag{3.40}$$

where AG_{max} is the equivalent of g_{syn}. We can use this equation to then fit simulation data using

$$G_{syn}(f) = R_n(f)AG_{max}\tau_1\tau_2 f \tag{3.41}$$

where this time we did not assume that the input rate is constant, rather we took its average value. Notice how STD changes the relation between input rate and average conductance from linear (Equation 3.31) to exponential (Equation 3.39, and Equation 3.41). In both cases however, the effect of the exponential term will diminish for higher input rates, and the relation will resemble a linear one. This is also evident in Figure 3.7,b&c where simulation data for both models are shown.

3.5 Cerebellum

Taking a closer look underneath the cerebral hemispheres one can find a smaller structure with a volume around a tenth of the overall brain. This structure is known as the cerebellum, which is Latin for "little brain". Surprisingly, even though the cerebellum is small, it accounts for more than half of the neurons in the brain (Kandel et al. 2000, ch. 42). Cerebellar neurons, highly regular and with repeating connectivity, receive projections from various brain and spinal cord areas, and project to different motor systems.

The cerebellum is organized in three distinct regions (Figure 3.8). The deepest region in called the granular layer, and contains granule cells, whose population is estimated to 100 billion, and Golgi cells. In some regions of the cerebellum small numbers of other cells can also be found in this layer, like Lugaro cells, unipolar brush cells and chandelier cells. This is also where the mossy fibres terminate, creating a synaptic complex called cerebellar

glomureli, that connects mossy fibres to both granule cells and Golgi cells (Figure 3.8, index)

In the middle, packed with the cell bodies of Purkinje cells, we can find the Purkinje cell layer. Purkinje cells constitute the output of the cerebellar cortex, and the main input of the cerebellar nuclei.

The outermost layer, also an important information processing layer, contains stellate cells and basket cells, along with Purkinje cell dendrites, and the granule cells axons, that run parallel to the long axis of the folia and thus called parallel fibres.

Functionally, the cerebellum is responsible for a large number of computational tasks, including the fine tuning of movements. As a result, patients with lesions in the cerebellum have various disruptions of normal movements, like moving their hand from a raised position to touch their nose with the tip of their finger. The cerebellum is also involved in smooth-pursuit eye movements and saccadic eye movements.
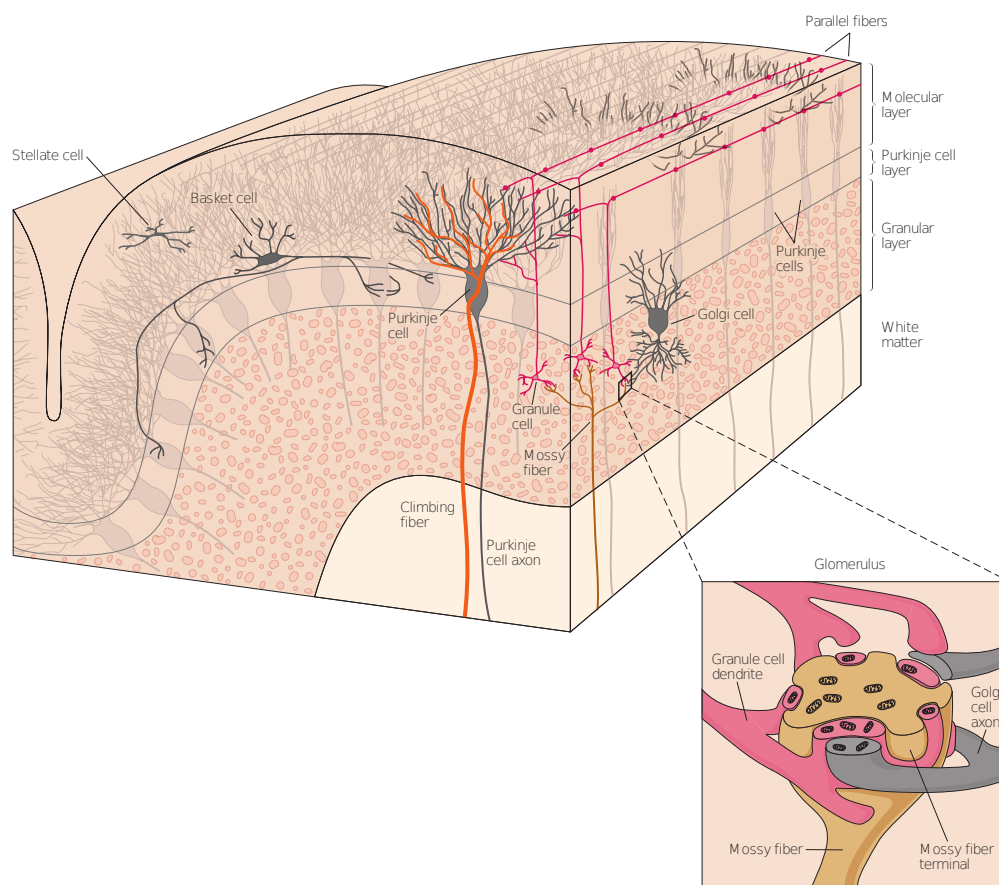
Figure 3.8: Cerebellar cortex. The cerebellar cortex consists of
three layers. The outer one, known as molecular layer, includes the
axons of the granule cells known as parallel fibres, the dendrites of
the Purkinje cells, stellate cells and basket cells. The intermediate
layer holds the somas of Purkinje cells, and is known as Purkinje
cell layer, while the inner layer consists of granule cells and Golgi
cells. Mossy fibres excite granule cells and Golgi cells by creating a
synaptic complex called the cerebellar glomerulus (index)

4

Effect of STD at excitatory synapses

Neurons act as computational devices, receiving both excitatory and inhibitory inputs from other neurons, and processing them simultaneously. Various factors and neuronal processes can affect the neuron's response to these inputs, and thus change the I–O function of the neuron. We focus here on the effect of short-term synaptic depression at the excitatory synapses of a neuron that receives both excitatory and inhibitory input.

In the presence of STD the amplitude of the post-synaptic conductance at individual synapses is scaled down by a factor, depending on the input rate. This can change the neuronal response significantly, lowering the effect of excitation at higher frequencies, and thus changing the neuron's I–O function. Since excitation results in an increase of the neurons output rate, STD can change neuronal gain by leaving the output rate unaffected for small input rates, while decreasing it for higher ones. Counter-intuitively , STD at the excitatory synapses can also change the effect that inhibitory
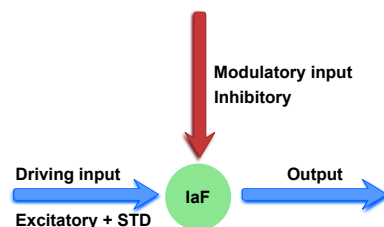
Figure 4.1: Inhibition-modulated neuronal output. We applied STD in the excitatory input, responsible for driving the integrate and fire neuron, while modulating the neuronal output using inhibitory input.

input has on the neuron.

Although not directly applied at the inhibitory synapses, STD at the excitatory synapse can affect the operation performed by inhibitory input. In particular, Rothman et al. (2009) showed that when a neuron is driven by excitation, applying depression to the driving input can have two effects. It changes the I–O function of the neuron, but most importantly, it can add a multiplicative component to the otherwise additive effects of the modulatory input.

To further investigate these effects, we first replicate the results described in Rothman et al. (2009) by stimulating an integrate-and-fire neuron with excitatory synaptic input, and comparing the different I–O functions in the presence and absence of STD. We then added tonic inhibition as modulatory input, and compared the effects of inhibition in the presence and absence of STD.

4.1   Integrate-and-fire neuron

We used an integrate-and-fire neuron to investigate how STD at an excitatory synapse could enhance inhibition-mediated gain modulation. Using the NEURON simulator (Carnevale T. and Hines L., 2006) we created a small soma whose length (L) and diameter (diam) equalled $9.76\,\mu$m, and that had $1\,\mu\mathrm{F}/cm^2$ capacitance (C_m), $100\,\Omega$·cm cytoplasmic resistivity and $386\,$pS of passive conductance (g_{pas}). These parameters had originally been chosen by Rothman and colleagues to represent cerebellar granule cells, which are small and electronically compact. As in Rothman et al. (2009),we used synaptic input at four excitatory synapses, each with a maximum conductance (g_{max}^{ampa}) of $1\,$nS, and tonic inhibitory input (g^{GABA}) of $500\,$nS to modulate the neuron. We recorded a spike when the neuron's voltage reached $V_{thres} = -49\,$mV , and set the voltage to $V_{spike} = 10\,$mV for an integration step to simulate a spike. We then set the voltage to the resting membrane potential $V_{rest} = -75\,$mV, and kept it there for a refractory period of $t_{ref} = 2.5\,$ms. A summary of these variables can be found in Table 4.1.

The excitatory synaptic impulse response was given by

$$G(t) = (1 - e^{-t/\tau_r})^n [a_1 e^{-t/\tau_{d1}} + a_2 e^{-t/\tau_{d2}} + a_3 e^{-t/\tau_{d3}}] \qquad (4.1)$$

where t is time, τ_r the rise time constant, and τ_{d1}, τ_{d2} and τ_{d3} the decay

Soma		Spike		Synaptic input	
Diam	$9.76\,\mu m$	V_{thres}	$-49\,mV$	n	4
L	$9.76\,\mu m$	V_{rest}	$-75\,mV$	g_{max}^{ampa}	1 nS
C_m	$1\,\mu F/cm^2$	V_{spike}	$10\,mV$		
g_{pas}	$128.6\,\mu S/cm^2$	t_{ref}	$2.5\,mV$	Tonic input	
				g^{GABA}	500.0 nS

Table 4.1: Biophysical properties of the integrate-and-fire neuron. Passive parameters of the IaF neuron along with the parameter we used for spike generation, and the properties of the synaptic excitatory, and tonic inhibitory input. Here excitation was used to drive the neuron, while inhibition was considered as the modulatory input. The membrane time constant is not needed for this simulation, but using Equation 3.10 we find $\tau_m = 7.7$ ms

n	11	α_1	2.23 nS	τ_{d1}	0.45ms
τ_r	0.10 ms	α_2	0.29 nS	τ_{d2}	2.88ms
δ	1 or 0.5	α_3	0.08nS	τ_{d3}	21.63ms

Table 4.2: Synaptic properties of the integrate-and-fire neuron. Synaptic parameters used in Equation 4.1 to simulate the post-synaptic response to excitatory synaptic input.

time constants. Depression was modelled as described in subsection 3.4.1, using the simpler Equation 3.33 with the depression factor (δ) equal to 1 in the absence, and 0.5 in the presence of STD, respectively. For the impulse response we used the same values as the ones calculated by Rothman et al. (2009), since they result from the fitting of the conductance equation to traces of AMPA receptor EPSCs. These values can be found in Table 4.2

We simulated the neuron using the backward Euler method for 10 s with a time step of 0.02 ms, and by calculating the average output rate for various excitatory input rates, we were able to determine the neuron's I–O function (the relation between input and output rate; Figure 4.2,blue). We then did the same in the presence of inhibitory input (Figure 4.2,red). To compare the two, we shifted the modulated I–O function by -10 Hz along the driving synaptic input axis, and noticed how the shifted curve (Figure 4.2,green) overlaid with the original one (Figure 4.2,blue). This means that the inhibitory input performs an additive operation. This has already been proposed by theoretical studies (Holt and Koch, 1997), and it has also been confirmed using a multi-compartmental model of a cerebellar nucleus neuron (Steuber

et al., 2011).
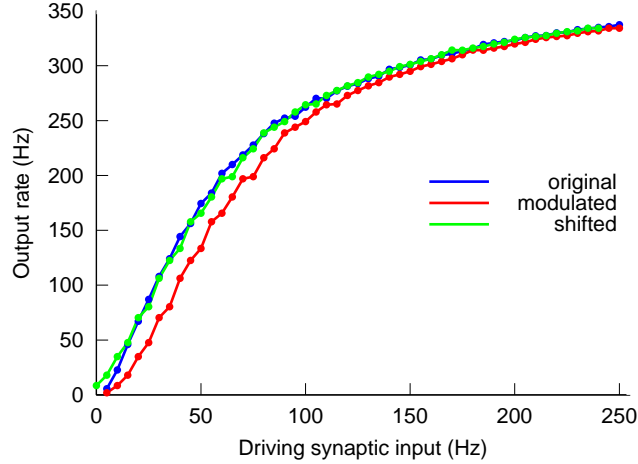
Figure 4.2: IaF I–O function. I–O function of an IaF neuron driven by excitatory input (blue). The biophysical properties of the neuron can be found in Table 4.1 and Table 4.2 . The original I–O function (blue) changed in the presence of modulatory input (red). To identify this change, we shifted the modulated function (red) by $-10\,\mathrm{Hz}$ along the input axis. The resulting curve (green) almost perfectly overlays the original one, indicating that modulatory input shifts the I–O function along the input rate axis, and thus performs an input additive operation .

Thus, by driving a neuron with excitatory synaptic input, we were able to use computational models of depression, and investigate its effects on the resulting I–O function, along with the changes in the arithmetic operation performed by the same input, in the presence and absence of depression.

4.2   Effect of short term depression

To replicate the effect of STD that had been studied by Rothman et al. (2009), we used the same depression model (Varela et al., 1997) where the actual response amplitude is given by the product of the maximum amplitude and a scaling factor (D). The scaling factors initial value is 1, multiplied by δ every time an input arrives; where $0 < \delta < 1$. Between stimuli, D recovered exponentially following the equation

$$\tau_D \frac{dD}{dt} = 1 - D \tag{4.2}$$

where the time constant τ_D was set to $300\,ms$.
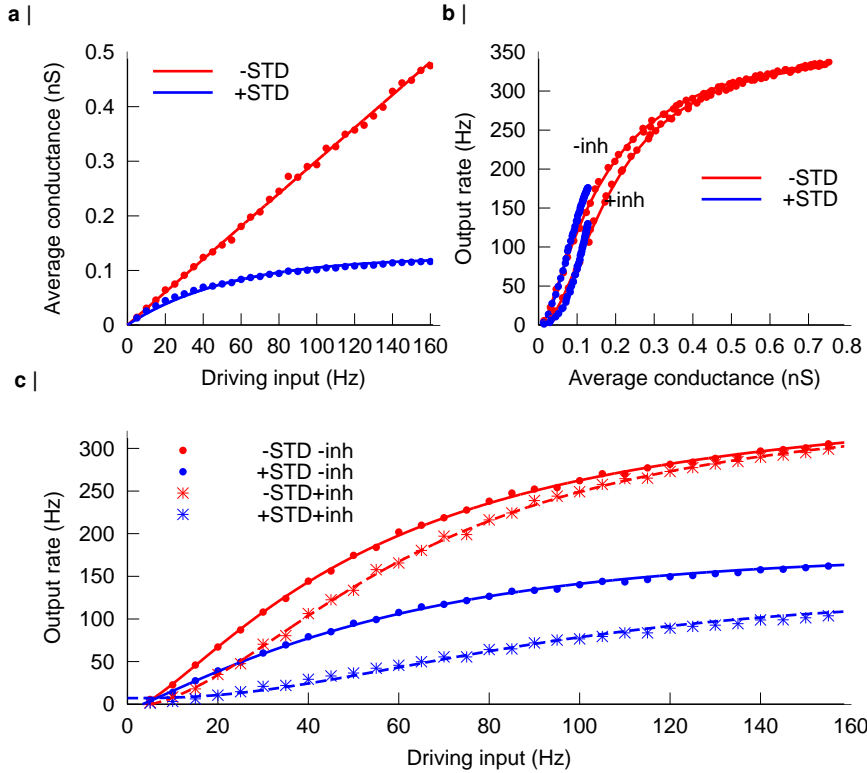
Figure 4.3: IaF neuron simulation data with and without STD. a | Average conductance for a single synapse as a function of the driving input rate, in the absence (red) and presence (blue) of STD. Dots correspond to simulation data, lines are fits to Equation 4.3 (red) and Equation 4.4 (blue). **b |** Output rate as a function of a synapse's average conductance in the absence (red) and presence (blue) of of STD; both for the presence (right curves) and absence (left curves) of modulatory inhibitory input. All lines are fits to Equation 4.5 Notice how this relationship remains largely unaffected by STD. **c |** I–O function in the presence (blue) and absence (red) of STD; and in the presence (*) and absence (.) of inhibitory modulatory input, along with the fits to Equation 4.6.

We ran the same simulation for $50\,ms$ before adding any stimuli, and then stimulated the model for $10\,s$, using synaptic excitatory input to drive the neuron , and tonic inhibitory input to modulate it. We did so using $\delta = 1$ and $\delta = 0.5$ to simulate the neuron in the absence and presence of depression, respectively. Apart from the I–O relationship we were also interested in the

relation between input rate and average conductance, and the relationship between average conductance and output rate. The simulation data for all three relationships are shown in Figure 4.3.

We used the fact that the I–O relationship is mediated by the average conductance, by calculating the average conductance from the input rate, and then using the calculated conductance value to find the output rate. Doing so we show how changes in the I–O function (Figure 4.3,c) are not generated by changes in the relation between average conductance and output rate, since both in the absence and in the presence of STD this relation remains the same (Figure 4.3,b). Rather they are a result of the non-linearity introduced by STD in the relationship between driving input and average conductance (Figure 4.3,a)

Since the I–O function is not linear, and consequently the gain is not the same for all values of the input rate, we relied on the average gain calculated over a specific output range,to identify multiplicative operations; while using the input rate corresponding to the half maximum output rate to denote additive ones. To do so though, and identify operations as in section 2.4, we had to use analytical equations that can adequately describe the underlying relations. We start with the relations between input rate and average conductance. In the absence of STD, this relationship is linear, and can be described by

$$G_{exc}^{lin}(f) = c_1 f \tag{4.3}$$

STD introduces a non-linearity, decreasing the response of the neuron to input rate for high input rates. For regular input, this relationship could be described using Equation 3.34, or Equation 3.40 if we used the STD model described in subsection 3.4.2. However, these equations would add to the complexity, so we used a simpler exponential function to fit our data instead. This function was

$$G_{exc}^{exp}(f) = c_2(1 - e^{-f/c_3}) \tag{4.4}$$

Using GNU octave (Eaton et al., 2009) and the Levenberg-Marquardt non-linear regression we fitted Equation 4.3 and Equation 4.4 to the simulation data (Figure 4.3,a and b) to describe both relations. We then need to use a sigmoid function to describe the relationship between conductance and

output rate. For that we worked as in Rothman et al. (2009), using the Hill function

$$F(G_{exc}) = \frac{F_{max}}{1 + |G_{exc}^{50}/G_{exc}|^n} + F_0 \tag{4.5}$$

Where F_{max}, G_{exc}^{50}, n and F_0 are constants that are found during the fitting process. Due to the intrinsic properties of this function, after fitting, F_{max} corresponds to the maximum difference from the minimum F_0 value, and G_{exc}^{50} to the conductance value where the output rate is in the middle of its range. These fits can be found in Figure 4.3,b. There we can see that, although STD changes the range of the function, resulting in a decrease of the maximum conductance value from 0.8 nS to approximately 0.13 nS, it does not change the shape of the curve substantially. As a result, curves in the presence and absence of STD overlay to a large extent.

To fit the I–O function, and take into consideration the non-linearity in the conductance as a function of input, we fitted Equation 4.5, substituting G_{exc} with equations Equation 4.3 and Equation 4.4, for simulation data in the absence and presence of STD, respectively (Figure 4.3,c). That is

$$I - O : F(G(f)) \tag{4.6}$$

After this fitting we were able to find the driving input that corresponded to a particular percentage of the output value. We denoted $F_{5\%}$, $F_{50\%}$ and $F_{75\%}$ the values of the 5%, 50% and 75% maximum output value, and $f_{5\%}$, $f_{50\%}$ and $f_{75\%}$ the input values that corresponded to these output values. Doing so we were able to define the average gain as

$$F' = \frac{F_{75\%} - F_{5\%}}{f_{75\%} - f_{5\%}} \tag{4.7}$$

and then calculate the gain difference using

$$\Delta Gain = \frac{F'_m - F'_o}{F'_o} \tag{4.8}$$

where F'_o and F'_m stand for the original and the modulated gain, respectively. In the same fashion, we define the offset as the input value that corresponds to the half maximum output value. That is

$$offset = f_{50\%} \tag{4.9}$$

The offset difference is then given by

$$\Delta offset = offset_m - offset_o \tag{4.10}$$

Both $\Delta Gain$ and $\Delta offest$ can be found in Figure 4.4. We can see that STD results in a gain decrease (Figure 4.4,b green bar), but only a minor decrease in offset (Figure 4.4,c green bar).

Most importantly, STD at the excitatory synapse can also affect the operation performed by inhibitory input. In the absence of STD, inhibition performs an additive operation, shifting the original I–O curve to the right (Figure 4.4,c red bar), without changing the gain (Figure 4.4,b red bar). On the other hand, in the presence of STD, inhibitory input does not only shift the I–O function (Figure 4.4,c blue bar) but also results in a gain change (Figure 4.4,b blue bar).
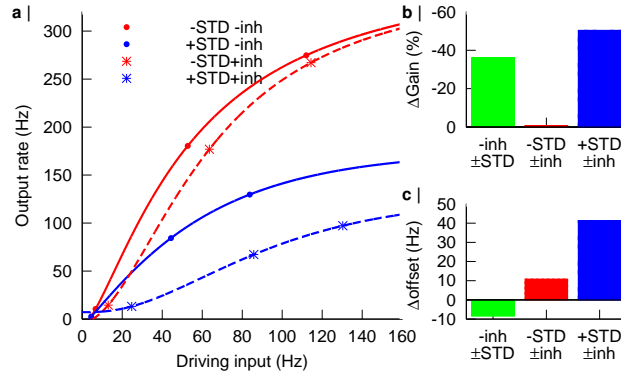
Figure 4.4: Gain and offset changes due to STD at an excitatory synapse. a | Fits of the I–O function using Equation 4.6, in the absence (blue) and presence (red) of STD, with (*) and without (.) inhibition. Stars and dots correspond to 5 %, 50 % and 75 % percent of the maximum output value, as found by the fitting. Same data as in Figure 4.3,c. **b |** Gain changes due to STD in the absence of inhibition (left); and due to the introduction of an inhibitory input both in the absence (middle) and presence (right) of STD. **c |** Offset changes for the same cases as in **b**.

4.3   Limitations

Fitting analytical functions to the data is crucial for identifying arithmetical operations, especially when the operations are not linear, and thus can not be described by a simple addition or multiplication in the data. Fitted equations help us to calculate the average gain or offset by allowing us to find the maximum value of the function. The maximum output rate value, in this case F_{max} in Equation 4.5, is hard to measure experimentally since it might correspond to a very high, and difficult to measure, input rate. Simulations are not limited in this fashion, since one can change input rate arbitrarily, but in extreme conditions the behaviour of the neuron may be different, and thus the increase of input rate might reduce the predictability of the model. This is why we rely on the fitted equation to find the maximum value. We need this value to find the 5% and 75% maximum values, and the corresponding input ones, and use it to disregard the beginning and the end of the curve. Having to extrapolate this maximum value poses the first limitation in our analysis.
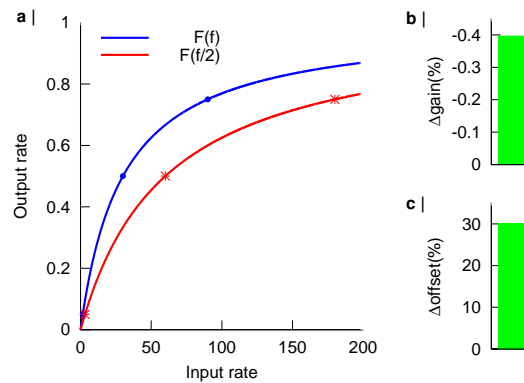
Figure 4.5: Offset limitations. a | Idealised neuronal response to input in the absence (blue) and the presence (red) of a modulatory operation. The latter results from an input multiplicative operation, given by Equation 4.12. Dots and stars correspond to the 5%, 50% and 75% of the maximum value. **b |** Difference in gain, calculated from Equation 4.8. **c |** Change in offset, as calculated from Equation 4.10. Notice that the above methodology reports an additive operation when an input multiplicative operation is performed.

The second caveat is that an offset change should not always be in-

terpreted as being the result of a linear input, or output, transformation. Multiplicative input operations might stretch the x axes, resulting in a dislocation of the $f_{50\%}$ value, without the need for an additive operation. To demonstrate this, we work with an idealised response of a neuron using

$$F(x) = \frac{1}{1 + {30}/{f}} \tag{4.11}$$

which is similar to the Hill function of Equation 4.5. When a modulatory input performs a multiplicative input operation, dividing the input rate by two, the I–O function of the modulated neuron is

$$F_{mod}(f) = F(f/2) \tag{4.12}$$

Using the same methodology as before, we calculate $\Delta Gain$ and $\Delta offset$ in Figure 4.5. What we notice is that along with the expected change in gain, we also find a change in the offset. This shows how gain changes can affect the offset measure that we use. As a result, even though average gain and offset as calculated here are good indicators of how an I–O function changes, one should also try to identify the underlying operation performed. Doing so for STD we find that it performs an input non-linear operation (section 5.4) that can account for the observed offset changes without the need for an additive operation.

5

Effects of STD at an inhibitory synapse

In the previous chapter we focused on the effect of STD in the excitatory driving input. This was studied before in cerebellar granule cells (GrC) (Rothman et al., 2009), receiving excitatory input from mossy fibres (MFs), and modulatory input from inhibitory Golgi cells (GoC). However, does STD have a similar effect when present at an inhibitory synapse? To find out, we used a biologically realistic model of a cerebellar nucleus (CN) neuron that already included STD at the inhibitory synapse from Purkinje cells. Since the output of the cerebellar cortex, and consequently the input to cerebellar nucleus neurons, comes from Purkinje cells (PCs) and is itself inhibitory, the cerebellar nucleus (CN) neurons can be viewed as inhibition driven, while receiving modulatory input from excitatory MFs (Steuber and Jaeger, 2013). As before, the responses of the CN neurons to driving input are depressed (Figure 5.1), since STD is present at the synapses from PCs to CN neurons (Pedroarena and Schwarz, 2003; Shin et al., 2007).

We investigated the role of STD for excitation-modulated neurons, using the CN neurons as a case study, but we also present results from an IaF neuron that is similar to the one we presented in the previous chapter. We were interested in both the effect that STD has on the I–O function of the neuron, and the effect on the operation performed by modulatory excitatory input.
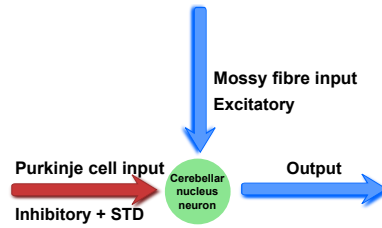
Figure 5.1: Excitation-modulated neuronal output. Cerebellar nucleus neurons receive inhibitory input from PCs, making them inhibition driven, while being modulated by excitatory input arriving from mossy fibres. Again STD is present in the driving input.

5.1   Cerebellar nuclei neurons

The Cerebellum is a particularly good model system for studying the effects of STD, because STD can be found at both excitatory (Rancz et al., 2007; Saviane and Silver, 2006) and inhibitory (Pedroarena and Schwarz, 2003; Shin et al., 2007) synapses. It is present at the excitatory synapse from MFs to GrCs, and at the inhibitory synapse from PCs to CN neurons. An IaF neuron with a connectivity that resembled the former was used in chapter 4 to investigate inhibition-mediated modulation, with STD present at the excitatory synapses. To investigate the excitation-mediated modulation, we focus on the CN neurons, where excitation is provided by MFs, and STD-exhibiting inhibitory synapses provide input from Purkinje cells (PC) (Figure 5.2).

We use a biologically realistic, conductance-based multi-compartmental model of the CN neuron (Steuber et al., 2011). This model divides the neuron in three distinct regions, the soma, the proximal dendrites, and the distal dendrites. Although some properties, like the axial resistivity ($Ra = 235.3\Omega{\cdot}cm$), capacitance ($Cm = 1.57\mu F/cm^2$) and passive membrane conductance ($28.1\mu S/cm^2$) remain constant through the neuron, others vary depending on their location.

In total, the CN model that we used had 517 compartments. Based on a published analysis of conductances in the CN (Steuber et al., 2011) eight types of ion channels were used. These were: two sodium channels, a fast and a persistent one; a fast and a slow delayed rectifier, Kv3 and Kv2 respectively; a high and a low voltage activated calcium channel; a tonic non
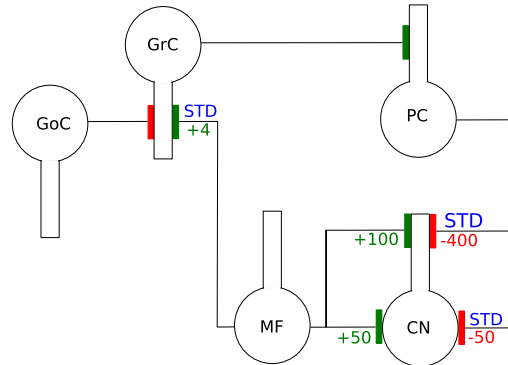
Figure 5.2: Simplified cerebellar connectivity. In the Cerebellum, GrCs receive excitatory input from mossy fibres (MFs) at synapses that exhibit STD, and inhibitory input from GoCs. On the other hand, CN neurons receive excitatory input from MFs, and STD is present in the inhibitory input arriving from PCs. Here, inhibitory and excitatory synapses are denoted with red and green, respectively, and the numbers correspond to the number of input received by our models in this and the previous chapter.

specific cation channel; a small conductance (SK) potassium channel that is calcium dependent; and a hyper-polarization activated cyclic-nucleotide gated (HCN) channel.

Synaptic input was provided by PC input to 450 inhibitory synapses, with 400 of them randomly placed on the dendrites, and 50 on the soma. Excitatory synapses received input from MFs, with 100 of them randomly placed on the dendrites, and 50 on the soma. Inhibitory synapses exhibited STD (Pedroarena and Schwarz, 2003; Shin et al., 2007), similar to the one found in Luthman et al. (2011), as described in subsection 3.4.1. The ISIs were generated as in Luthman et al. (2011) using

$$\text{ISI} = (1 - x)y + xyz \tag{5.1}$$

where y is the mean ISI, and z is random number between zero and one that follows a third order gamma distribution. Irregularity is controlled by x, which can take a value from zero, where input is regular, to one, where input is irregular with the same distribution as in z. GABAergic synapses from PCs to CN neurons were modelled as bi-exponential synapses with

$\tau_{rise} = 0.25$ ms and $\tau_{fall} = 5.1$ ms, while synapses from MFs to CN neurons were modelled using three different bi-exponential synapses. An AMPA ($\tau_{rise} = 0.29$ ms and $\tau_{fall} = 4.01$ ms) a fast NMDA ($\tau_{rise} = 2.87$ ms and $\tau_{fall} = 11.6$ ms) and a slow NMDA ($\tau_{rise} = 2.87$ ms and $\tau_{fall} = 78.3$ ms).
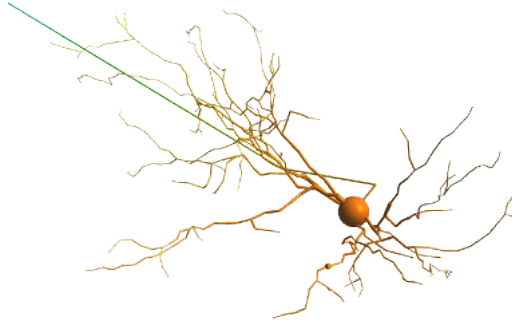
Figure 5.3: Morphology of the cerebellar nucleus model neuron. Soma and dendrites can be seen in orange, and the axon in green.

5.2   Short term depression at inhibitory synapses enables gain modulation

We used a previously published, biologically realistic, conductance based model (Steuber et al., 2011) to investigate the role of short-term synaptic depression at the inhibitory synapse between Purkinje cells and cerebellar nucleus neurons. We were interested in the effect STD had on the input output relationship (I–O). To identify this effect, we simulated neuronal activity for various rates of the inhibitory driving input, thus finding the I–O relationship. We did so for two different levels of modulatory excitatory mossy fibre input, 20 Hz and 50 Hz; and in the presence and absence of STD.

To analyse the result, we worked as before, assuming that the I–O relationship is mediated by the average conductance. We thus first studied the relationship between inhibitory input f and average conductance G_{inh} in the absence of STD. This relationship is linear, and can be described using

$$G_{inh}^{lin} = c_1 f \tag{5.2}$$

where c_1, along with c_2 to c_7 introduced bellow, are constants, whose

exact value is found by fitting the corresponding equation to the simulation data. In the presence of STD, this relationship changes to an exponential. To identify this relationship we fitted our simulation data to the equation

$$G_{inh}^{exp} = c_2(1 - e^{-f/c_3})$$ (5.3)

Both data and results of the fitting can be found in Figure 5.4, left.

We then identified the effect of STD in the output firing rate (F) as a function of the average conductance relationship. To do so we fitted a Hill-like function in the simulation data.

$$F(G_{inh}) = \begin{cases} c_4 / \left(1 + \frac{c_5}{|c_7 - G_{inh}|^{c_6}}\right) & c_7 - G_{inh} > 0 \\ 0 & else \end{cases}$$ (5.4)

The results are shown in Figure 5.4,b. Notice that the two curves overlay, and depression has a negligible effect on this relationship. This effectively means that changes in the I–O function are a result of the non-linearity introduced by STD in the relation between average conductance and input rate.

However, the relationship we are most interested in is the relationship between input and output rate (Figure 5.5, a), especially with regards to gain changes due to the presence of STD. To identify these gain changes, we fit Equation 5.4, only this time substituting G_{inh} with $G_{inh}(f)$, using Equation 5.2, and Equation 5.3 appropriately. That is

$$F(f) = F(G_{inh}(f))$$ (5.5)

We used the equations above to calculate gain, using two points of this function that corresponded to 5% and 75% of the maximum output rate. We denoted these points as $p_{5\%}(f_{5\%}, F_{5\%})$ and $p_{75\%}(f_{75\%}, F_{75\%})$, with f and F representing the input and output rate respectively. We calculated changes in gain and offset as in chapter 4, using

$$F'(f) = \frac{F_{75\%} - F_{5\%}}{f_{75\%} - f_{5\%}}$$ (5.6)

to calculate the gain, while the offset was defined as the input rate that corresponded to the half maximum output rate. That is
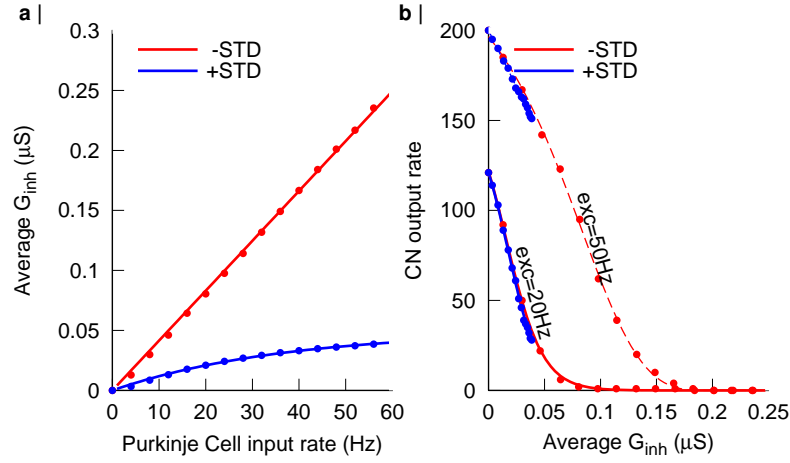
Figure 5.4: Effect of inhibitory STD on the I–O function.
a | Average inhibitory conductance as a function of inhibitory input rate in the absence (red) and presence (blue) of STD. Dots and lines correspond to simulation data and fits to Equation 5.3 (blue) and Equation 5.2 (red), respectively. **b |** Output rate as a function of G_{inh} for excitatory input of 20 Hz and 50 Hz. Notice how the curves overlay in the presence and absence of STD. Lines are fits to Equation 5.4.

$$offset = f_{50\%} \tag{5.7}$$

We then calculated the percentage change in gain as

$$\Delta Gain = \frac{F'_m - F'_o}{F'_o} \tag{5.8}$$

Where F'_o and F'_m denote the gain in the original and modulated function, respectively. The change in offset was found by subtracting the already calculated values.

$$\Delta offset = offset_m - offset_o \tag{5.9}$$

We calculated the difference in gain and offset for various cases (Figure 5.5) and found two different effects. Firstly we found that for excitatory modulatory input of 20 Hz the presence of STD resulted in a gain change, along with a change in offset (top and bottom green bars, respectively). We then investigated the effect that STD at the inhibitory synapse had on
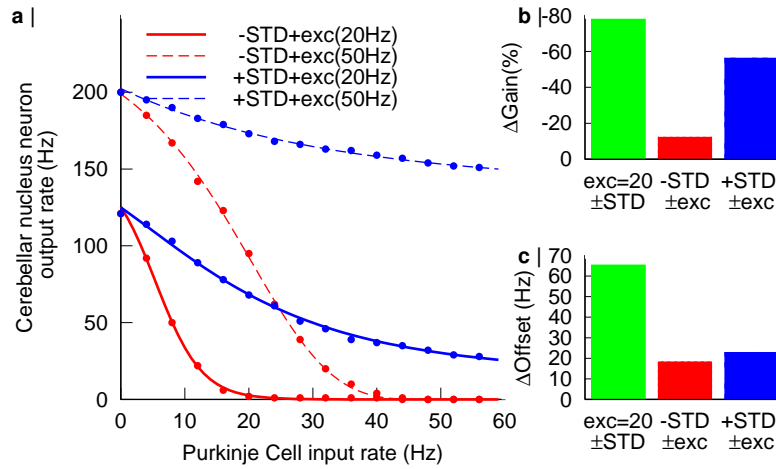
Figure 5.5: Inhibitory STD introduces gain modulation. **a |**
Average output rate of the CN neuron as a function of PC inhibit-
ory input rate, for 20 Hz and 50 Hz of excitatory MF input. Dots
and lines correspond to simulation data and fits to Equation 5.5,
respectively. **b,c |** Change in gain (**b**) and offset (**c**) in the presence
and absence of STD for 20 Hz of excitatory input (green bars); and
for a change of the excitation from 20 Hz to 50 Hz in the absence
(red bars) and presence (blue bars) of STD.

the transformation performed by excitatory input. To do so, we increased
the excitatory modulatory input from 20 Hz to 50 Hz, and compared the
transformation of the I–O functions. In the absence of STD increasing the
excitatory input resulted in an offset change, and a minor gain change (Fig-
ure 5.5,b and c red bars); while in the presence of STD excitatory input
again increased the offset, but also resulted in a substantial gain change
(Figure 5.5,b and c blue bars). Our second finding is thus that STD at the
inhibitory synapse can account for changes in the transformation performed
by input at the excitatory synapse.

Out of these two effects, it is the second one that is the most interesting.
As before, STD at one synapse affects the operation performed by the other
synapse. To explain this behaviour, one should first understand the way in
which STD transforms the I–O function; something we discuss in section 5.4.

5.3   Integrate-and-fire neuron

To demonstrate that gain modulation in a CN neuron is not limited to the specific biologically realistic neuron model, we repeat the simulations using an IaF neuron model, similar to the one used in section 4.1. We changed the reversal potential of the synaptic input from 0 mV to -75 mV to simulate the inhibitory driving input, and the reversal potential of tonic input from -75 mV to 0 mV to simulate the excitatory modulatory input.
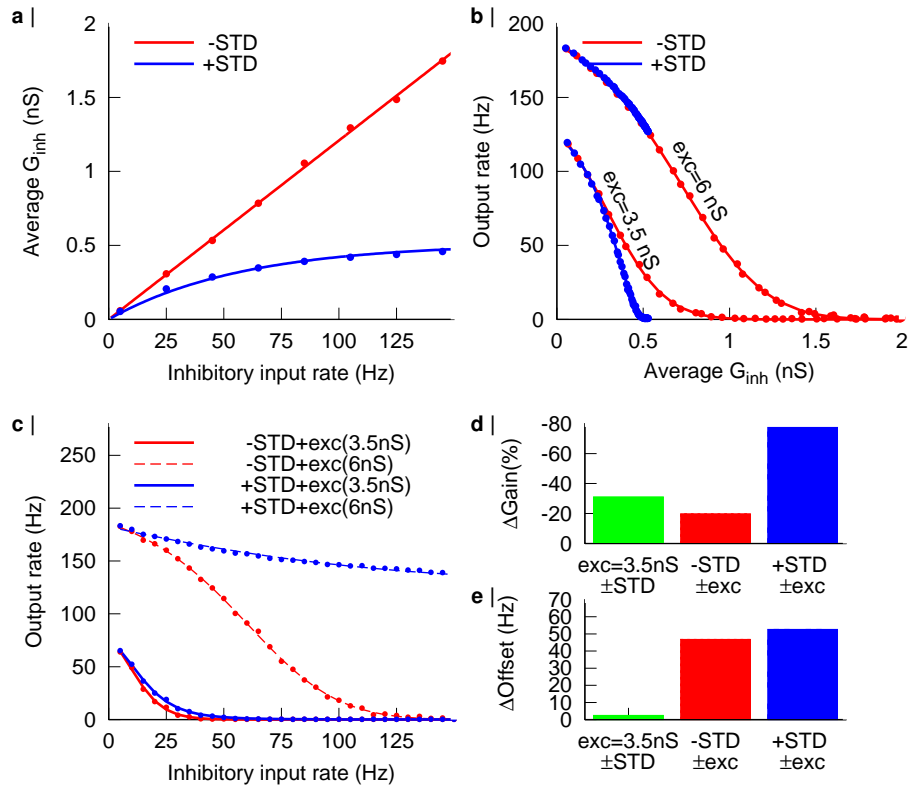
Figure 5.6: Gain modulation at an excitatory mediated IaF neuron. a | Average conductance as a function of input rate in the absence (red) and presence (blue) of STD. **b |** Output rate as a function of average conductance in the absence (blue) and presence (red) of STD, and for 3.4 nS and 6 nS of excitatory input. **c |** I–O function 3.4 nS and 6 nS of excitatory input in the absence and presence of STD. **d,e |** Change in gain (b) and offset (c) for three distinct cases. For the presence and absence of STD for 3.5 nS of excitatory input (green bars); for a change of the excitation from 3.5 nS to 6 nS in the absence (red bars) and presence (blue bars) of STD.

We used the same methodology as in the previous section, and again noticed that STD induced a change in the average conductance as a function of input rate, while leaving the output rate as a function of average conductance largely unaffected (Figure 5.6, a and b).

Contrary to CN neurons, which receive input from 450 inhibitory synapses, this IaF neuron receives input from just four. This slightly affects the output rate as a function of average conductance, which does not perfectly overlay in the presence and absence of STD. Even so, the effect of STD on gain modulation remains the same, and STD in the inhibitory input introduces excitation mediated gain control (Figure 5.6, d blue bar compared to red bar).

5.4 STD operations

To understand how gain modulation can arise from the introduction of STD, we must first understand the transformation performed by STD. In particular, we focus on the non-linearity imposed by STD in the average conductance as a function of input rate, and how this non-linearity can translate to changes of the I–O function. This is important, especially since the output rate as a function of average conductance remains unaffected by STD, meaning that changes in the conductance as a function of input rate can solely account for changes in the I–O function (Figure 4.3,b;Figure 5.4,b).

Transformations in the average conductance are the same as the transformation of the I–O function when both are seen as input operations. Inputs operations were first discussed in section 2.1, and correspond to changes in the input of a particular function. In particular, for a function $f(x)$, an input operation g transforms the input in the following manner

$$f'(x) = f(g(x))$$

shifting the function horizontally, along the input rate axis. A similar non-linear shift can describe changes in the average conductance as shown in Figure 5.7.

Input operations in the average conductance can account for changes in the I–O function. As we can see in Figure 5.7, STD shifts the data point that corresponds to 10 Hz of synaptic input by 40 Hz along the input rate axis. The same transformation is performed in the I–O function. Notice how
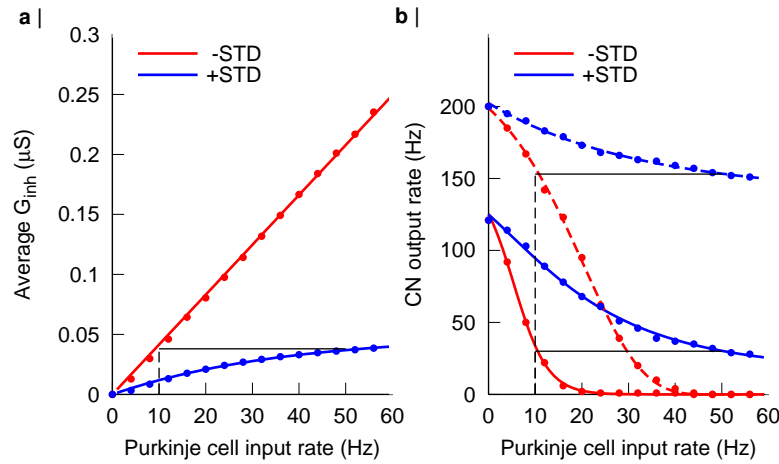
Figure 5.7: STD performs an input operation. a | Average
conductance as a function of input rate. In the presence of STD,
50 Hz of input rate will result in the same average conductance as
10 Hz of input rate in the absence of STD. STD will thus shift the
point that correspond to 10 Hz by 40 Hz along the input rate axis
(as indicated by the black line). **b |** Output rate as a function of
input rate. The effect of STD on the I–O function is the same as it
was for the average conductance (a). For both 20 Hz and 50 Hz of
excitatory modulatory input, STD will shift the point corresponding
to 10 Hz of inhibition by 40 Hz along the input rate axis.

this transformation of the average conductance, and thus the I–O function,
in non-linear. This means that as the input rate increases, the horizontal
distance between the red (-STD) and blue (+STD) curve in Figure 5.7, left
will increase.

However, the selection of an input operation is also supported by the
biophysics of STD. As shown in section 3.4, STD depresses the input of
the synapse, changing the conductance value, and consequently the value of
the average conductance. If we disregard the conductance fluctuations due
to synaptic input and assume that synaptic input affects only the average
conductance, the decrease of average conductance due to STD is equivalent
to a decrease of input rate. This is a fair assumption to make especially for
neurons that receive input from multiple sources, since due to superposition
they are less subject to conductance fluctuations (Figure 3.6). Function-
ally, this translates to an input change on the I–O function, thus the input
operation is supported both numerically and biophysically.

Having identified the transformation performed by STD, we can now proceed to explain how this transformation can lead to gain changes, and in particular how it can change the transformation performed by excitatory input.

5.5   Origin of STD dependent gain control

Identifying the operation performed by STD we unravelled the effects of STD on the I–O function, but this does not answer the question how STD can allow changes in one synapse to affect the operation performed by another, and in particular how it can induce gain control. A major contribution of this work, is the elucidation of that mechanism.

In particular, to explain how STD at the inhibitory synapse can change the transformation performed by excitatory input, we use an idealised I–O function, along with modulatory input that shifts the I–O function along the input rate axis as proposed by theory (Holt and Koch, 1997). We assume that the neuron was driven by inhibition and modulated by excitation, and that the I–O function is a reversed sigmoid. As before, we use inputs resulting in 5%, 50% and 75% of the maximum output rate to calculate gain and offset as in Equation 5.6 and Equation 5.7, respectively. Notice how this time, we report *gain* and *offset*, and not $\Delta gain$ and $\Delta offset$.

Starting from the original and modulated I–O function, and assuming that the average conductance is linear, we apply three distinctive input transformations to the average input conductance: a linear one (Figure 5.8,a), a simple non-linear one (Figure 5.8,b), and an exponential similar to the one performed by STD (Figure 5.8,c). We next apply the same input transformations to the I–O function, since as we saw in the previous section, the input transformation in the average conductance as a function of input rate accounts for all changes in the I–O function.

The linear transformation of the average conductance as a function of input rate represents STD that is independent of the input rate, or a simple change of weights. In the top panel of Figure 5.8,a we can see the original idealised I–O rates in red both without (solid line) and with (dashed line) modulatory input.
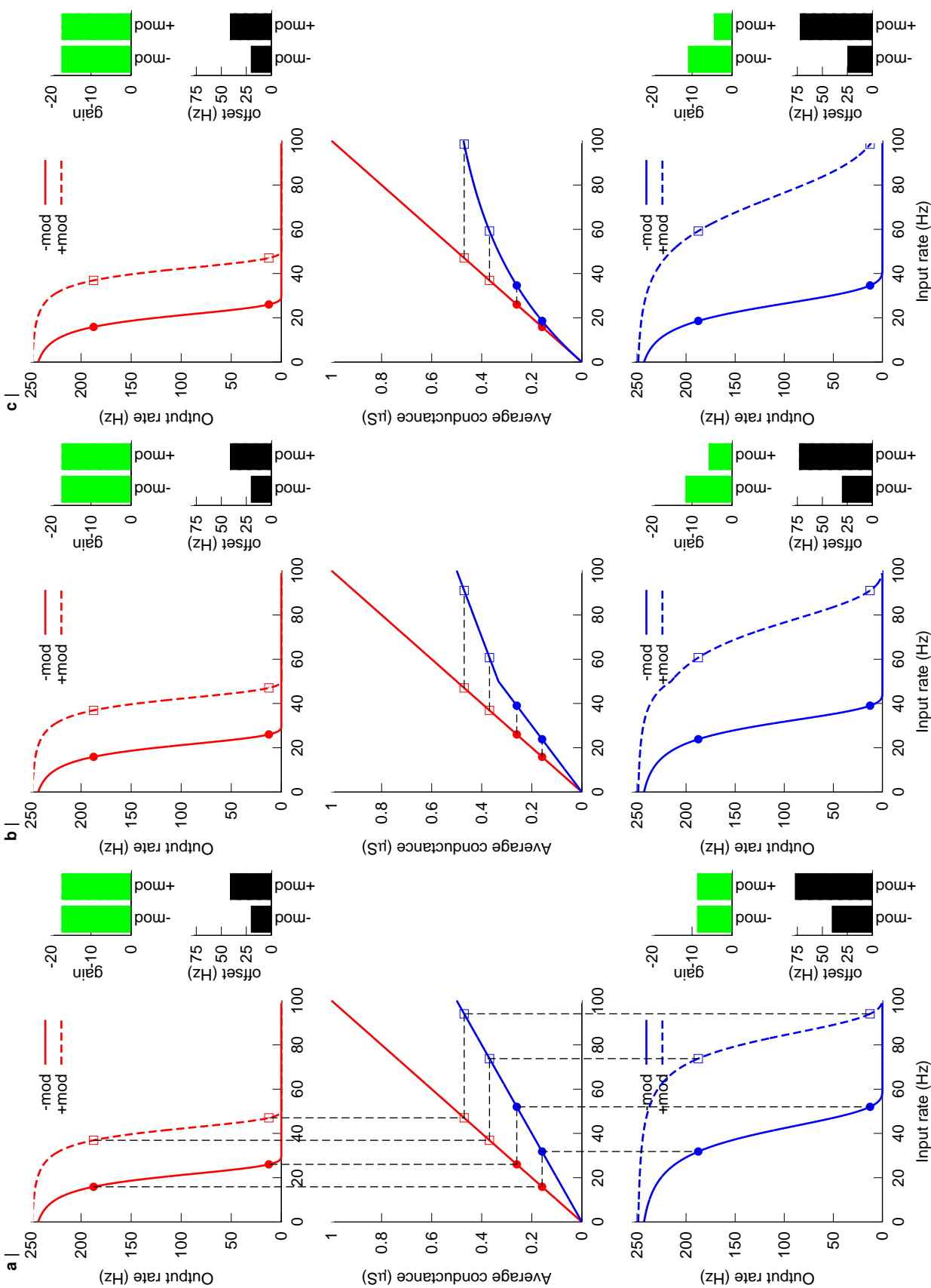
Figure 5.8: Idealised STD effects on gain. a,top | Idealised responses of a neuron driven by inhibitory input ranging from 0 Hz to 100 Hz, in the absence (red solid) and presence (red dashed) of excitatory modulatory input, along with the points corresponding to 5% and 75% of maximum output rate, in the absence (dots) an presence (squares) of modulatory input. These points are used to calculate gain (green bars) as the average slope. Offset (black bars) is calculated as the input rate that corresponds to the half maximum output value. **a,middle |** Idealised transformation of the average conductance as a function of input rate, where the original curve (red) undergoes a linear multiplicative input change (blue). This will result in the same transformation performed in the I–O curve. Here we can see how this transformation affects the data points for a input rate that corresponds to 5% and the 75% of the maximum output rate; both in the absence (red dots to blue dots) and presence (red squares to blue squares) of modulatory input. **a,bottom |** The idealised neuronal response transformed as a result of the transformation in the average conductance, along with the gain and offset calculated as above. Notice how the gain has changed, but this change remains the same for both the unmodulated and the modulated I–O function. **b |** Same as in **a**, but with the introduction of a tilt in the transformation of the average conductance as a function of input rate (middle) and consequently in the transformation of the I–O functions (bottom). Notice how the non-linearity changes the gain effect of the transformation depending on the input range where the original I–O function is situated. If the original I–O function is situated after the tilt, the undergoing gain change is bigger. This can result in the change of the overall transformation performed by the modulatory input, adding a multiplicative component to the otherwise purely additive operation. **c |** Same as in **a** and **b**, for a transformation similar to the one performed by STD.

The transformation performed can be seen in the middle panel, where the original average conductance (red) has undergone a multiplicative operation (blue). The same transformation is performed in both I–O functions. The result can be seed in the bottom panel, for the absence (solid) and presence (dashed) of modulatory input. The transformation results in a change in both gain and offset, but the operation performed by the modulatory operation remains additive. We can notice this since, both before and after the transformation, the gain of the unmodulated and modulated I–O function

remains the same (green top and bottom bars).

The mechanism that allows the modulatory input to perform gain control is apparent in the second case, where we used a simple transformation, tilting the transformed average conductance to create a simple non-linearity (Figure 5.8,b middle). Although artificial, this simple non-linearity is good for demonstrative purposes. As we can see the subsequent transformation of the I–O function has different effects depending on the input range the original I–O function lies in. For the original I–O curve, left of the introduced tilt, the transformation leads to a smaller gain change, compared to the gain change introduced by the modulated function, right of the tilt.

As a result, effects introduced by this transformation are variable, leading to bigger gain changes when the I–O function lies at higher input rates, in such a way that the transformed values lie past the introduced tilt. Having understood how a simple non-linear operation can lead to a gain change we can move to more realistic transformations.

The last transformation we used was similar to the one performed by STD (Figure 5.8,c). Here, the average conductance as a function of input range takes a form similar to Equation 5.3. Again, the transformation has a different effect on both the conductance and the I–O function depending on the corresponding input rate. For higher input rates, this transformation results in a different gain change, with higher input rates that result in bigger gain changes. Since modulatory operations shift the I–O rate along the input rate axis, and towards higher input rates, they also shift them towards a range where the input transformation has a different effect. As a result, a multiplicative component is added to the overall transformation performed by modulatory input.

5.6   Input and output operations

Having briefly described how gain modulation can arise from STD, we proceeded to formalise the use of input operations. To do so we use the three relations described so far. These were the average conductance as a function of input rate, the output rate as a function of average conductance, and finally the output rate as a function of input rate.

We start by formalising the change in the relation between average conductance and input rate using an input operation. We start by fitting the

relation between average conductance and input rate in the absence of STD using the linear Equation 5.2

$$G_{inh}^{lin}(f) = c_1 f$$

only this time instead of using Equation 5.3 to fit the average conductance as a function of input rate in the presence of STD, we use an input operation. To do so we define

$$mod(f) = f - c_2 * (e^{f/c_3} - 1) \tag{5.10}$$

and use it to modulate input

$$G_{inh}^{+STD}(f) = G_{inh}^{lin}(mod(f)) \tag{5.11}$$

The results, along with the calculated $mod(f)$ function can be seen in Figure 5.9, a&b.

To see if the modulation in average conductance can account for changes in the I–O function, we work as before to find the equations that can describe the relation between average conductance and input rate, and the I–O function. That is, we use the Hill equation applied before (Equation 5.4) to our data to describe the relation between output rate and average conductance $(G_{inh}(f))$ in the absence of STD for both 20 Hz and 50 Hz of modulatory input (Figure 5.9,d), and then use Equation 5.5 $(F(f) = F(G_{inh}(f)))$ to calculate the I–O function for both cases .

Knowing these two relations, we modulate the input of these functions using $mod(f)$ in a way similar to the one used in Equation 5.11. That is

$$F(f) = F\left(G_{inh}^{lin}(mod(f))\right) \tag{5.12}$$

The results can be seen in (Figure 5.9,c).

As we can see, describing the changes in average conductance as an input operation can also account for changes in the I–O function. On the other hand our simulations were performed using asynchronous irregular input, and for a large number of inputs. This means that there were no large voltage fluctuations, and as a result the overall output relied mainly on the average conductance. However, this is not always the case. Limited amount of input, regular input, and synchronous input, can change the

relation between average conductance and output rate. This can add a
second operation to the overall I–O function, and thus affect the performed
gain change. Although it is not possible to calculate gain changes for all
cases, we are going to consider some of them in the next chapter.
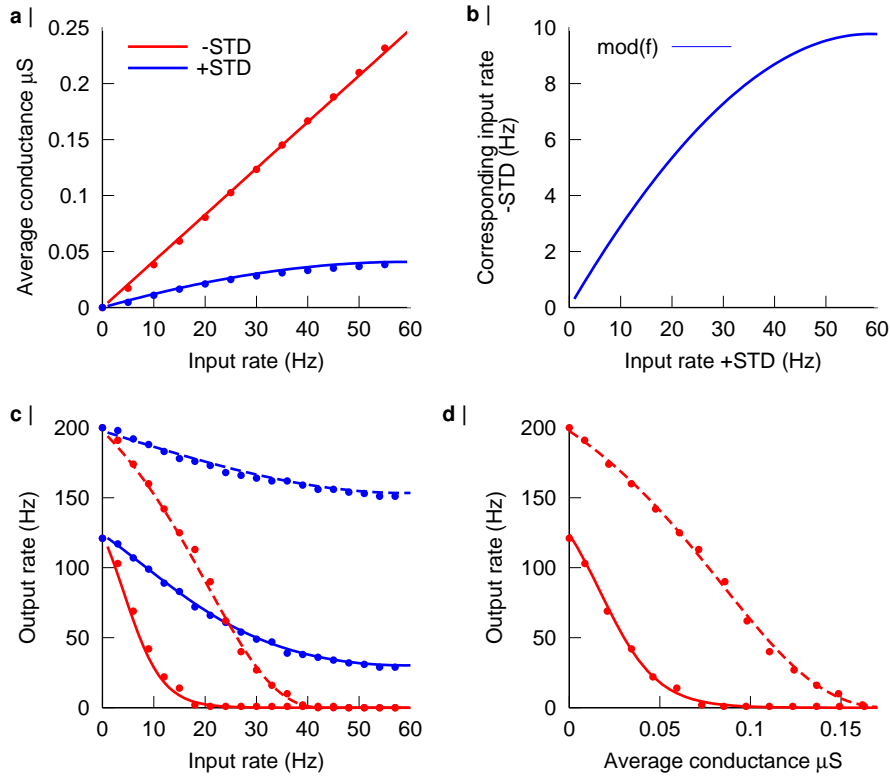
Figure 5.9: Modulated I–O function. a | Simulation data
(dots) of the average conductance as a function of input rate in the
absence (red) and presence (blue) of STD, along with the fits to
Equation 5.3 and Equation 5.11, respectively. **b |** Relation between
the input rate in the presence of STD, and the input rate that cor-
responds to the same output rate in the absence of STD, given by
Equation 5.10. **c |** Simulation data (red dots) and fits (red lines)
of the I–O function in the absence of STD, along with simulation
data in the presence of STD (blue dots) and the corresponding I–O
functions (blue lines). The modulated I–O functions were found
by modulating the input using Equation 5.10, and then using the
modulated input as in Equation 5.11. Solid and dashed lines corres-
pond 20 Hz and 50 Hz of modulatory excitatory input, respectively.
d | Output rate as a function of average conductance for 20 Hz
(bottom) and 50 Hz (top) of modulatory input, along with fits to
Equation 5.4.

6

Determinants of gain modulation

In the previous chapter, we investigated the effect of STD at an inhibitory synapse, and found that it changes the gain, and that it enables excitatory modulatory input to further modulate gain in a multiplicative manner. Here we use control simulations to investigate the robustness of this result against parameter variations in our model. To do so we change various aspects of our experiment, and calculate gain changes to find that STD enabled gain control persists. Since we simulate neuronal activity using realistic neurons, there are a number of biological parameters that can be altered to identify changes arising from the introduction of STD, but two of them stand out.

The first one is related to STD itself. In particular, can different levels of STD affect the observed gain changes? To investigate this we ran the same experiment as before for varying STD levels (section 6.1). The model we used for the original simulations was introduced in Shin et al. (2007), and it assumed that the depression level changes are due to changes in the pre-synaptic release probability. To simulate varying various levels of STD we introduced a depression coefficient and used both positive and negative values to simulate both depression and facilitation.

The second deviation from the original model is not related to the neuron itself, but rather to the type of input (section 6.2). Originally, we used asynchronous irregular input to investigate the effect of STD. To investigate how different input types can change the effect of STD, we use a combination of synchronous, asynchronous, regular and irregular input.

6.1   Varying levels of STD

Depression of inhibitory input at the inhibitory synapses of the CN neurons
was simulated using a model first described in Shin et al. (2007) (subsec-
tion 3.4.2). This model assumed that there is a steady-state value of the
release probability (R_{ss}) that depends on the input rate (f), and that is
given by

$$R_{ss}(f) = 0.08 + 0.60e^{-2.84f} + 0.32e^{-0.02f}$$

where the constants were found by fitting the equation to experimental data
from Pedroarena and Schwarz (2003). To simulate varying levels of STD,
we extended the model by adding a depression coefficient c to modulate the
extent of depression. In this new version of the model R_{ss} was given by

$$R_{ss}(f) = 0.08 + 0.60e^{-2.84cf} + 0.32e^{-0.02cf} \tag{6.1}$$

We used positive and negative c values to simulate different STD levels,
where successive synaptic activation depresses neuronal response, and dif-
ferent short term facilitation (STF) levels, where consecutive inputs en-
hance neuronal response, respectively. For the default level of STD we used
$c = 1$, which corresponded to the experimental verified case, along with
$c = 1/100$ and $c = 1/200$ for intermediate STD levels. To invert the direc-
tion of plasticity and simulate facilitation, we used $c = -1/200$, $c = -1/100$
and $c = -1/70$. The effects of these changes on the I–O function can be
found in Figure 6.1. To identify gain changes due to various STD and STF
levels, we used a procedure similar to the one described in section 5.6.

We started by fitting a linear function to the relation between input
rate and average conductance in the absence of STD or STF (red curve in
Figure 6.1,a). As before we used

$$G_{inh}^{lin}(f) = c_1 f \tag{6.2}$$

where f is the input rate and c_1 the fitted constant. We then used an input
operation to describe the operation performed by STD and STF. We did
not use Equation 5.10, since it was not capable of describing the relation for
both STD and STF. Instead, we used
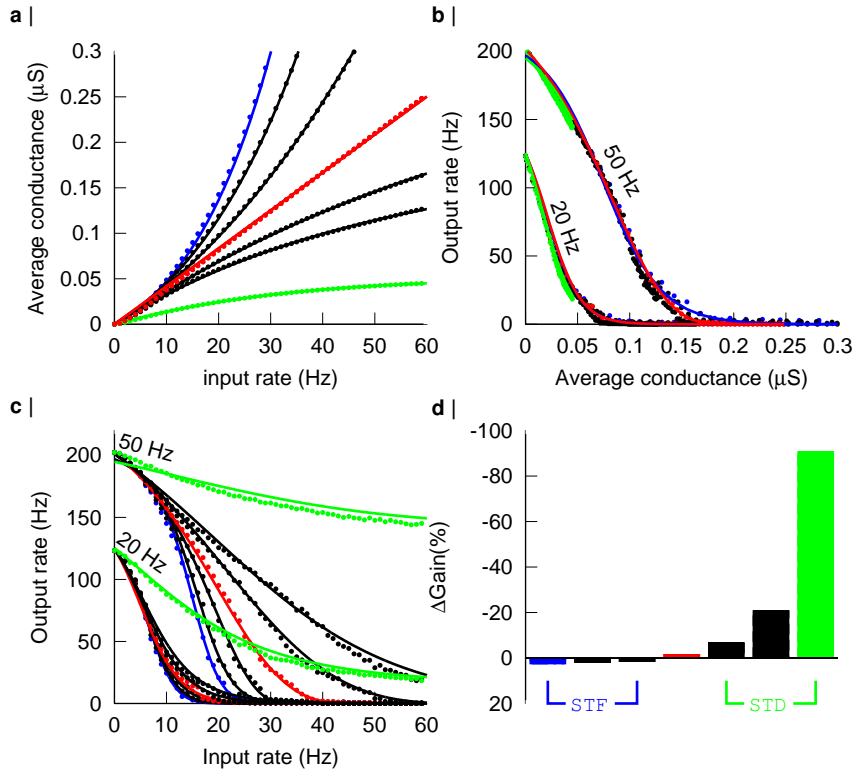
**Figure 6.1: Gain modulation due to varying STD and STF
levels. a |** Average conductance in the presence of STD (green),
in the absence of STD and STF (red), and in the presence of STF
(blue); intermediate levels of both STD and STF are shown in black.
Dots correspond to simulation data of the CN neuron model, and
lines are fits to Equation 6.2 and Equation 6.4 for the absence and
presence of plasticity, respectively. **b |** Output rate as a function
of average conductance for the same cases as in **a.**, and for 20 Hz
and 50 Hz excitatory input. Lines are fits of a Hill function (Equation 5.4) . Notice how the blue, red, and green curves overlay.
Intermediate STD and STF levels were omitted for clarity. **c |** I-O
function for the same cases as **b**. Lines are fits to Equation 6.5 and
Equation 6.6 for the absence and presence of plasticity, respectively.
Notice how STD and STF will have a greater effect on the gain of
the top curves, which correspond to 50 Hz of excitatory input. **d |**
Gain changes due to the increase of modulatory input from 20 Hz to
50 Hz as measured by Equation 5.8, in the presence of STF (blue),
in the absence of plasticity (red),and in the presence of STD (green),
along with gain changes for intermediate plasticity levels (black).

	c	+STD			No Plasticity	+STF		
		1	$\frac{1}{100}$	$\frac{1}{200}$	-	$-\frac{1}{200}$	$-\frac{1}{100}$	$-\frac{1}{70}$
Equation 6.3	$c_1(\cdot 10^{-3})$	4.18	4.18	4.18	4.18	4.18	4.18	4.18
	c_2	0.99	0.99	0.95	0	1.00	1.07	1.10
	$c_3(\cdot 10^{-5})$	2.76	2.23	519.7	$1 \cdot 10^5$	352.40	4.45	1.31
	$c_4(\cdot 10^{-3})$	1.36	1.10	.002	0	-15.5	$-.002$	$-.01$
Equation 5.4	c_4	160	157	157	157	153	153	169
	c_5	12	12	10	10	9	9	10
	c_6	765	760	621	621	638	652	653
	c_7	12	12	10	10	10	10	10

Table 6.1: Fitting parameters for different levels of STD and STD. Fitting coefficients for various values of c, corresponding to STD, STF, and the absence of plasticity. Notice how Equation 5.4 was fitted for every c, resulting in seven different Hill function sets, all with similar values.

$$mod(f) = f \cdot (|c_2 + c_3 f|)^{c_4} \tag{6.3}$$

which was capable of describing changes due to both STD and STF as an input operation. In effect, the average conductance (G) as a function of input rate (f), in the presence of STD and STF was given by

$$G_{inh}^{+STD}(f) = G_{inh}^{lin}(mod(f)) \tag{6.4}$$

The fits of Equation 6.2, and Equation 6.4 to our simulation data can be found in Figure 6.1,a.

As before, we can notice that the relation between average conductance and input rate remains largely unaffected by STD and STF (Figure 6.1,b). We fit this relation with a Hill function (Equation 5.4), and again we combine the two relations to find the output rate as

$$F(f) = F\left(G_{inh}^{lin}((f))\right) \tag{6.5}$$

in the absence of plasticity, and

$$F(f) = F\left(G_{inh}^{lin}(mod(f))\right) \tag{6.6}$$

in the presence of it.

As we can see the input transformation, given in Equation 6.3, used to describe changes in the average conductance as a function of input rate (Equation 6.4 and Figure 6.1,a), can also account for changes in the I–O function (Equation 6.6 and Figure 6.1,c). Notice how for 20 Hz of modulatory input rate, all the I–O functions start from the same point, and there is no significant deviation from the non-plasticity case, denoted in red. On the other hand, for 50 Hz of modulatory input rate, the I–O function has the same value for 0 Hz input, but now the deviation increases with input rate. This clearly shows that plasticity at the inhibitory synapse can change the transformation performed by the excitatory synapse, adding a multiplicative component that changes the gain depending on the level of depression or facilitation. The effect of plasticity on the gain changes can also be seen in Figure 6.1(d) where the percentage gain difference was calculated based on Equation 5.8 for the various plasticity levels. Notice that the y axis is reversed, and increasing facilitation increasing gain changes, while depression decreases them.

6.2 Input regularity and synchronicity

The pattern of input a neuron receives can influence its I–O function. For synaptic input, synchronicity (Person and Raman, 2012; Oviedo and Reyes, 2002) and regularity (Luthman et al., 2011) have been found to affect neuronal response. This is why we chose to repeat our experiments using different synchronicity and regularity levels. Although this will obviously have an effect on the neuronal response, we were interested in identifying the effect of STD, that is, the introduction of a gain change, and most importantly, the enabling by STD of the excitation-mediated gain control.

6.2.1 Regularity

The input used so far in our model did not have any temporal regularity. So for every input rate in simulations done in previous chapters, the instantaneous input rate did not remain the same throughout the simulation; rather noise was introduced so that the inter-spike intervals would follow a third order gamma probability distribution. Here, we investigated the effects of this noise, and thus irregular input, on the I–O function of the CN neurons, especially with regards to the operations performed by STD. More
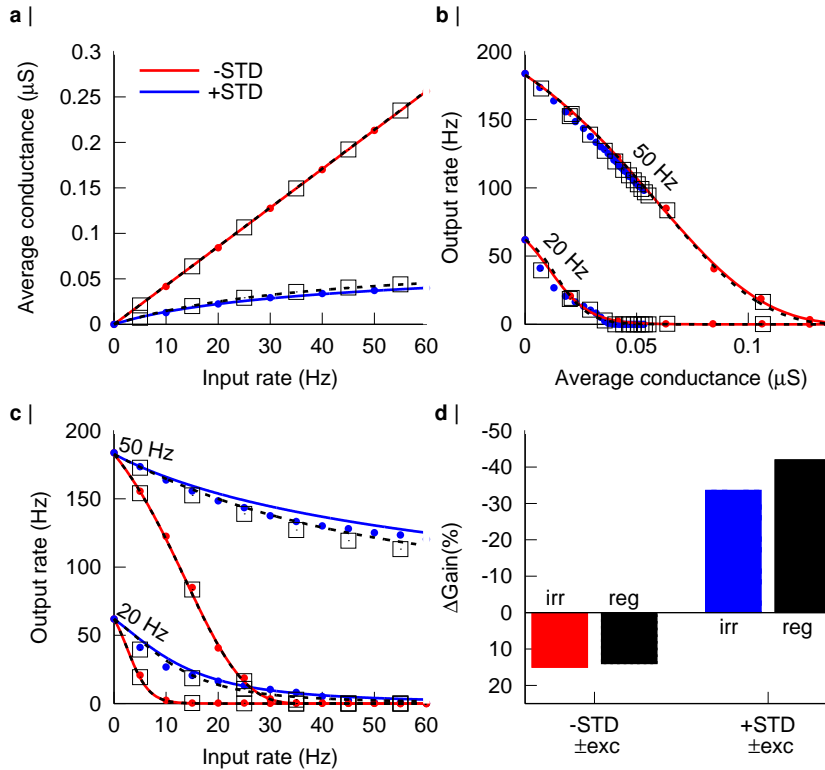
Figure 6.2: Effect of regularity. Comparison between regular and irregular input. Notice that some data points and fitted curves can not be seen, as they perfectly overlay with others. **a** | Average conductance as a function of input rate for irregular input in the absence (red) and presence (blue) of STD. Dots correspond to simulation data and the red and blue lines are fits to Equation 6.2 and Equation 6.4, respectively. The corresponding simulation data and fits for regular input are plotted as black boxes and black dashed curves. **b** | Output rate as a function of average conductance for irregular input in the absence (red) and presence (blue) of STD, and for 20 Hz and 50 Hz excitatory input. Dots correspond to simulation data and all curves are fits to a Hill equation (Equation 5.4). As in **a**, black boxes and curves are the corresponding data points and fits for asynchronous input. **c** | I–O function in the absence (red) and presence (blue) of STD. As in **b**, coloured plots and points, and black plots and points, correspond to irregular and regular input, respectively. **d** | Percentage gain change (ΔGain) due to the increase of excitatory input from 20 Hz to 50 Hz for both irregular (irr) and regular (reg) input, and in the presence and absence of STD. Notice how in both cases STD decreases the gain in the operation performed by the excitatory input.

specifically, we were interested in identifying if the percentage gain change, introduced by STD to the operation performed by excitation, was affected by changes in regularity.

We worked as before, only for two distinct cases. In the first one we generated irregular PC input following a third order gamma probability distribution by setting $x = 1$ in Equation 5.1, while in the second we used $x = 0$ to generate regular PC input. In both cases MF input was asynchronous and irregular ($x = 1$). Fitting the average conductance as a function of input rate using a linear (Equation 6.2) , and a non-linear (Equation 6.4) equation for simulations that correspond to the absence and presence of STD, respectively. As we can see in Figure 6.2(a), regularity does not play a role in this relation, since the curves that correspond to irregular (blue and red) and the regular (black) input patterns overlay.

We found a similar result for the relation between output rate and average conductance. As we can see in Figure 6.2(b) for both 20 Hz and 50 Hz excitation, STD does not play any role since we can fit the same Hill function (Equation 5.4) in both the absence (red) and presence (blue) of STD. This holds for both irregular (red and blue) and regular (black) input.

Not surprisingly, since both relations remain unaffected, so does the I–O function. Although the overlay of the I–O function is not perfect in Figure 6.2(c), the deviations are minor. Using $F(G(0))$ as the maximum, and $F(G(120))$ as the minimum output rate values we calculated the percentage change in average gain (ΔGain) using Equation 5.6 and Equation 5.8. Notice that for both regular and irregular input, STD introduces a substantial gain change in the operation performed by excitatory input (Figure 6.2,d).

This result was expected, mainly since the model we used received input from 450 PCs. Due to superposition, the conductance trace will be a sum of all the synaptic responses, and as a result changes in noise are not expected to have a substantial effect. This is understandable if you consider that for every point in time, a response that is greater due to an input arriving later, cancels out with a response that is lower due to an input arriving sooner. This means that regularity should only play a role if we have a very small number of inputs, or if input applied at different synapses is synchronous.

6.2.2   Synchronicity

To investigate the effects of synchronicity we changed the input of our model
so that the input from all PCs arrived at the same time. Doing so, we ran
simulations for inputs that were both regular, and irregular. In this way we
were able to examine the effect of synchronicity, but also to investigate the
effect of regularity during synchronous input. Most importantly, we were
interested in investigating the effect of STD during synchronicity, and find
out if STD at the inhibitory synapse still enabled excitation to perform gain
control.

   Although synchronicity changes the conductance trace introducing large
voltage fluctuations, the average conductance as a function of input rate re-
mains the same, as shown in Figure 6.3(a), where data have been fitted using
(Equation 6.2) for the linear, and (Equation 6.4) for the non-linear case. On
the other hand synchronicity has a profound effect at the relation between
average conductance and output rate, and it makes the neuron respond dif-
ferently in the presence and absence of STD. This is evident in Figure 6.3(b),
where all the curves correspond to fits to a Hill function (Equation 5.4).
Here, for both 20 Hz and 50 Hz excitatory input, the curves corresponding
to the absence and presence of STD do not overlay. This means that changes
in the I–O function will not be the sole result of changes introduced in the
average conductance as a function of input rate. However, neither do the
curves that correspond to synchronous irregular and synchronous regular
input overlay, indicating that when input is synchronous, regularity has an
effect on neuronal response.

   By fitting a Hill function (Equation 5.4) to describe the relation between
output rate and average conductance, and substituting for the conductance
as found for the absence (Equation 6.5) and presence (Equation 6.6) of
STD, we can again find the 5% and 75% maximum values. To do so, we
use $F(G(0))$ as the maximum, and $F(G(200))$ as the minimum output rate
values. We notice that in both cases the percentage gain change in the
absence of STD is bigger that the percentage gain change in the presence of
STD.

   Even though synchronicity can affect gain, having a profound effect on
the operation performed by excitation, STD still decreases gain changes
induced by the modulatory operation (Figure 6.3,d, right bars, compared
with left bars). However, this decrease is not the same for synchronous

irregular input (Figure 6.3,d blue bar compared to red bar),and synchronous regular input (Figure 6.3,d right black bar compared to left black bar). Notice how for synchronous irregular input the decrease is not big enough for excitation to performed a gain decrease (blue bar), but this is mainly because in contrast to previous cases, the initial effect of excitation largely increases the gain (red bar). The interaction between the effect of synchronicity and the effect of STD are yet to be investigated.
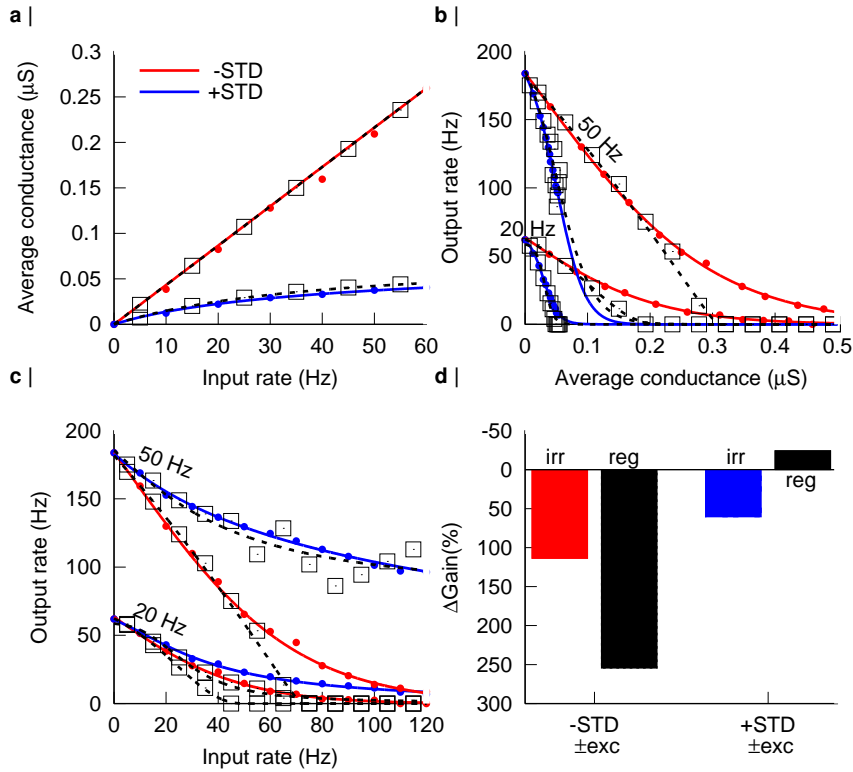
Figure 6.3: Effects of synchronicity. Effects of synchronous irregular, and synchronous regular input. **a** | Average conductance as a function of input rate for synchronous irregular input and for the absence (red) of presence (blue) of STD, along with the corresponding function for synchronous irregular data (black boxes and dashed curves). Lines are fits to Equation 6.2 and Equation 6.4, respectively. **b** | Output rate as a function of average conductance for 20 Hz and 50 Hz of excitatory input. Red and blue lines are fits to a Hill function (Equation 5.4) in the absence and presence of STD and for synchronous irregular input, respectively. Black lines are the corresponding fits for synchronous regular input. **c** | I–O function for synchronous irregular input in the absence (red) and presence (blue) of STD, along with the corresponding curves (black) and data (boxes) for synchronous regular input. **d** | Percentage gain change (ΔGain) , for both irregular (irr) and regular (reg) input, due to the increase of excitatory input from 20 Hz to 50 Hz, and in the presence and absence of STD. Notice how in this case, regularity affects ΔGain (left bars). However, for both synchronous irregular and synchronous regular input, the introduction of STD will decrease the gain change performed by excitatory input (right bars, compared to left bars).

6.3 Synchronicity evokes time-locked spiking

In the process of identifying the STD effect on CN neurons, we realised that synchronicity has an interesting effect on the I–O function. As seen in Figure 6.3,c, the presence of synchronicity increases the distance of the simulated points from the fitted hill function, and produce a saw-tooth like effect. That is, the output rate of the neuron is not always decreasing as inhibitory input increases, rather for some ranges an increase in inhibitory input leads to an increase in the neuron's output rate.

To investigate this effect, we ran simulations using the same model and found that this effect persisted for various excitation levels and in the presence and absence of STD. We identified this effect to be a result of time-locked spiking resulting, something that has already been experimentally verified in CN neurons receiving synchronous input from PCs in mice (Person and Raman, 2012). We investigated only the effect of synchronicity between PCs, since these have indeed been found to exhibit synchronous activity in vivo (Heck et al., 2007; de Solages et al., 2008). Since spike time-locking was not in the scope of this thesis, we did not investigate it thoroughly, but rather use a simple example here to give a brief explanation.

As before, we use the CN model in the presence of STD and for 40 Hz of synchronous, regular excitatory input to modulate the neuron, even though different modulation levels did not change our results. Simulating for 5 sec, and for synchronous, regular inhibitory increments of 1 Hz we get the neuron's I–O curve (Figure 6.4,left). Once again, input and output rate are time-locked for various parts of the curve, where the output rate is proportional to the input rate. Consequently, there are parts of the I–O curve where increasing inhibitory input will increase the output rate.

To demonstrate how this is possible, we plot the GABAergic conductance trace along with the voltage trace for 55, 65, 75 and 85 Hz of inhibitory input (red, green, cyan and magenta traces Figure 6.4,right, black traces correspond to GABAergic conductance). The corresponding points in the I–O curve are also shown (red, green, cyan and magenta dots in Figure 6.4,left). As we can see, for 55 Hz of inhibition the output rate is twice the input rate, since the output rate lies on $F(f) = 2f$, with F and f corresponding to the output rate and input rate, respectively.

Taking a closer look at the voltage trace (red) for 55 Hz we see the
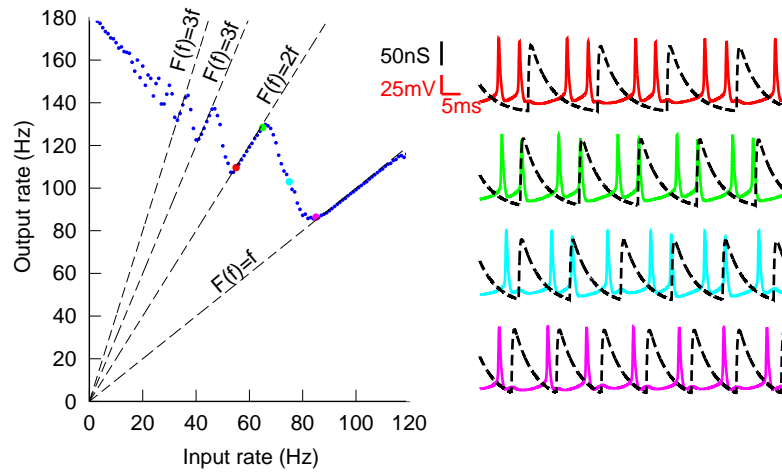
Figure 6.4: Synchronicity enables neurons to time-lock their spiking. **Left |** I–O function for a CN neuron receiving 40 Hz of synaptic excitatory input from MFs in the presence of STD. Differently coloured points correspond to 55 Hz (red), 65 Hz(green), 75 Hz(cyan) and 85 Hz(magenta) of inhibitory input. **Right |** Voltage trace for 55 Hz (red), 65 Hz(green), 75 Hz(cyan) and 85 Hz(magenta) of inhibitory input, along with the corresponding GABAergic conductance. Notice how for 55 and 65 Hz the neuron fires twice after every synaptic activation, while for 85 Hz, the neuron has a single respond after every synaptic activation.

output rate is twice the input rate, and thus 110 Hz because two spikes occur between two consecutive inhibitory activations. Increasing inhibitory input to 65 Hz (green), the output rate is still twice the value of the input rate, and thus 130 Hz. This is because the time window between two inhibitory activations decreased, but still barely allows for two spikes (green trace). Thus the output rate is time locked to the input rate, and increases with the increase of the inhibitory input. A further decrease of the time window between GABAergic activations (that is increasing inhibitory input rate) results in the elimination of the second spike. For 75 Hz of inhibition, almost half of the second spikes have been eliminated (cyan trace). This trend continues until all second spikes are eliminated, and the CN neuron has again time locked its spike with the PCs input, producing a single spike after every activation of the inhibitory synapses (85 Hz, magenta trace).

7

Discussion

Neurons can use a multitude of methods to process information. These methods are not necessarily limited to the inner workings of the neuron, since they can also relate to the way neurons receive or transmit information. In many cases, both in the peripheral nervous system (Adrian and Zotterman, 1926) and in the cortex (London et al., 2010), the overall result of neuronal information processing is the transformation of input rate to output rate. Since neurons can use their spike rate to encode information (chapter 2) the output rate as a function of input rate, also known as the I–O function, plays a major role in neuronal processing.

Intrinsic neuronal processes or input from other neurons can affect a neuron's I–O function in various ways, one of them being by changing its slope. The change or control of the slope of the I–O function is known as gain modulation or gain control, respectively. As we saw in chapter 2, gain modulation can play diverse roles, and it can result from a wide variety of mechanisms. It is also noticeable that apart from the I–O rate function, slope changes in other relations between stimulus parameters such as retinal position, orientation or contrast and output rate (Figure 2.2, Murphy and Miller, 2003), and between driving currents and output rate (Chance et al., 2002) have also been studied.

Setting aside the various functional roles of gain control discussed in chapter 2, there is another reason why gain modulation is so important: it changes the basic computations performed by neurons. If there is no change in slope, changes in the I–O function, or in any of the functions discussed in the previous paragraph, are limited to shifts along the input or the output

axis. Effectively, the computations capable of producing these shifts are limited to additive and subtractive operations (Silver, 2010). On the other hand the presence of gain modulation indicates underlying multiplicative operations, increasing the computational potential of a single neuron. In effect, the presence of gain modulation complements neuronal processing, and enables the use of all four basic operations by the neuron. That is, input addition and multiplication, and output addition and multiplication.

As it was not possible in the present thesis to investigate all possible mechanisms responsible for gain control, our research has concentrated on the question how short-term synaptic plasticity can enable gain modulation. This has been studied before for excitatory synapses (Rothman et al., 2009), but here we focused on inhibitory synapses, and more specifically on the inhibitory synapse from PCs to CN neurons in the cerebellum. We have made two contribution to knowledge: firstly, that STD at an inhibitory synapse can enable gain modulation, but most importantly, we have identified the transformation performed by STD, and we have demonstrated how this particular transformation can lead to gain modulation. The underlying mechanism of STD based gain modulation, along with its known limitations is discussed in the next section.

7.1 The mechanism of STD-dependent gain modulation and its limitations

Synaptic depression reduces neuronal responses to a particular input, and consequently changes the neurons I–O function. With STD having an increasing effect at higher input spike rates, it is not surprising that STD will change the slope of the I–O curve. On the other hand enabling gain modulation in a different synapse, and not the synapse STD is applied to, is remarkable. As is often the case, this counter-intuitive behaviour is a result of a simple mechanism. STD can indeed change the I–O function introducing a gain change, but this change is not always the same. Rather, the amount of gain modulation STD will induce depends on the part of the input rate axis the I–O function lies on. When a modulatory input is applied to the neuron, it usually results in a shift of the I–O function. Only if STD is present, this shift will move the I–O function towards an input rate where STD has a different effect; resulting in a change of the STD effect. This

means that STD at one synapse can change the operation performed by a different input, adding a multiplicative component to the otherwise additive effect.

But the mechanism responsible for the introduction of gain modulation has limitations. As synaptic properties can change with temperature (Person and Raman, 2012), so with the effect of STD, and given that less STD is observed at physiological temperatures, STD dependent gain modulation might be less prominent in behaving animals than in brain slices. Another limitation is intrinsic to the non-linear nature of the operation responsible for gain modulation. Although the transformation performed is non-linear, the degree of non-linearity changes depending on the input rate. A good example of this can be seen in Figure 6.1,a. There, if the green curve corresponding to the STD case is viewed from 0 Hz to 40 Hz, the non-linearity is evident. However, when limited to values greater than 40 Hz, the relation resembles a linear one.

7.2 Future work

Having identified the effects of inhibitory STD, and how it can enable gain modulation raises several other scientific questions.

First and foremost, it is important to have an experimental verification of the simulation results. Although similar results were found at an excitatory synapse, experimental data would increase our confidence into the presented theory and provide the ultimate proof of the effect of inhibitory STD on gain modulation. These data could either be data for any inhibitory synapse that exhibits STD, enhancing our overall understanding of the underlying processes, but data for the particular synapse from PCs to CN neurons are preferable.

However, STD is not the only mechanism capable of changing the I–O function. As we saw in chapter 6, input conditions, like regularity and synchronicity, can also affect the I–O function. In the present thesis we have discussed some of them, and showed how in their presence gain modulation might change, but the overall effect of STD persists. Although it is not possible for someone to investigate the effects of STD under all possible input conditions, neuronal properties, and variety of input sources, our understanding of how STD can affect neuronal output can increase if experiments

under various conditions unveil aspects of the discussed mechanism that are yet unknown. Moreover, having identified how a non-linearity can affect the neuronal output, it is worth trying to identify other non-linearities that might have similar effects.

Last but not least, the question remains about the functional roles of STD. Knowing the effect of STD on a single cell, can we find the effect it will have on networks? Will it affect working memory, where STD has a strong effect (Mongillo et al., 2008), and how does it contribute to the temporal response characteristics of V1 neurons (Chance et al., 1998)? Finally, apart from the link that STD has with tottering mice (Luthman et al., 2011; Steuber and Jaeger, 2013), are there any other STD contributions to motor control? These questions are not limited to the cerebellum, however, since STD is present in multiple areas of the brain, finding the functional roles of STD in other brain areas is equally interesting. In any case, one can conjecture that STD will have regulatory effects, since when present at a synapse it can decrease its effects, while simultaneously controlling the operation performed by other inputs. It can thus control neuronal functions depending on the input frequency, allowing neurons to act as multiplicative devices at lower frequencies, and transforming them to additive devices at higher frequencies.

Bibliography

Abbott, L. F., Varela, J. A., Sen, K., and Nelson, S. B. (1997). Synaptic Depression and Cortical Gain Control. *Science*, 275(5297):221–224. 34

Adrian, E. and Zotterman, Y. (1926). The impulses produced by sensory nerve endings Part 3. Impulses set up by Touch and Pressure. *The Journal of physiology*, 61(4):465–483. 25, 101

Andersen, R. A., Essick, G. K., and Siegel, R. M. (1985). Encoding of spatial location by posterior parietal neurons. *Science*, 230(4724):456–458. 27, 28, 34

Andersen, R. A. and Mountcastle, V. B. (1983). The influence of the angle of gaze upon the excitability of the light-sensitive neurons of the posterior parietal cortex. *The Journal of Neuroscience*, 3(3):532–548. 27, 28

Anderson, J. S., Lampl, I., Gillespie, D. C., and Ferster, D. (2000). The Contribution of Noise to Contrast Invariance of Orientation Tuning in Cat Visual Cortex. *Science*, 290(5498):1968–1972. 27, 30

Azouz, R. (2005). Dynamic Spatiotemporal Synaptic Integration in Cortical Neurons: Neuronal Gain, Revisited. *Journal of Neurophysiology*, 94(4):2785–2796. 30

Betz, W. J. (1970). Depression of transmitter release at the neuromuscular junction of the frog. *The Journal of Physiology*, 206(3):629. 33

Bialek, W., Rieke, F., de Ruyter van Steveninck, R., and Warland, D. (1991). Reading a neural code. *Science*, 252(5014):1854–1857. 25

Billings, G., Piasini, E., Lorincz, A., Nusser, Z., and Silver, R. A. (2014). Network Structure within the Cerebellar Input Layer Enables Lossless Sparse Encoding. *Neuron*, 83(4):960–974. 19

Borg-Graham, L. J., Monier, C., and Fregnac, Y. (1998). Visual input evokes transient and strong shunting inhibition in visual cortical neurons. *Nature*, 393(6683):369–373. 30

Bower, J. M. and Beeman, D. (2014). *The Book of Genesis: Exploring Realistic Neural Models with the General Neural Simulation System.* 22, 40

Brenner, N., Bialek, W., and de Ruyter van Steveninck, R. (2000). Adaptive rescaling maximizes information transmission. *Neuron*, 26(3):695–702. 19, 27

Brotchie, P. R., Andersen, R. A., Snyder, L. H., and Goodman, S. J. (1995). Head position signals used by parietal neurons to encode locations of visual stimuli. *Nature*, 375:232–235. 28, 34

Capaday, C. (2002). A re-examination of the possibility of controlling the firing rate gain of neurons by balancing excitatory and inhibitory conductances. *Experimental Brain Research*, 143(1):67–77. 30

Carandini, M. and Heeger, D. J. (1994). Summation and division by neurons in primate visual cortex. *Science*, 264(5163):1333–1336. 30

Carnevale T., N. and Hines L., M. (2006). *The NEURON Book.* 22, 40, 62

Cash, S. and Yuste, R. (1998). Input summation by cultured pyramidal neurons is linear and position-independent. *The Journal of neuroscience*, 18(1):10–15. 30

Cash, S. and Yuste, R. (1999). Linear Summation of Excitatory Inputs by CA1 Pyramidal Neurons. *Neuron*, 22(2):383–394. 30

Chance, F. S., Abbott, L. F., and Reyes, A. D. (2002). Gain modulation from background synaptic input. *Neuron*, 35(4):773–782. 30, 31, 34, 101

Chance, F. S., Nelson, S. B., and Abbott, L. F. (1998). Synaptic depression and the temporal response characteristics of V1 cells. *The Journal of neuroscience : the official journal of the Society for Neuroscience*, 18(12):4785–99. 53, 104

de Solages, C., Szapiro, G., Brunel, N., Hakim, V., Isope, P., Buisseret, P., Rousseau, C., Barbour, B., and Léna, C. (2008). High-Frequency Organization and Synchrony of Activity in the Purkinje Cell Layer of the Cerebellum. *Neuron*, 58(5):775–788. 99

Destexhe, A. and Paré, D. (1999). Impact of Network Activity on the Integrative Properties of Neocortical Pyramidal Neurons In Vivo. *Journal of Neurophysiology*, 81(4):1531–1547. 30

Destexhe, A., Rudolph, M., and Pare, D. (2003). The high-conductance state of neocortical neurons in vivo. *Nat Rev Neurosci*, 4(9):739–751. 30

Dittman, J. S., Kreitzer, A. C., and Regehr, W. G. (2000). Interplay between facilitation, depression, and residual calcium at three presynaptic terminals. *The Journal of Neuroscience*, 20(4):1374–1385. 53

Doiron, B., Longtin, A. A., Berman, N., and Maler, L. (2001). Subtractive and Divisive Inhibition: Effect of Voltage-Dependent Inhibitory Conductances and Noise. *Neural Computation*, 13(1):227–248. 30, 34

Eaton, J. W., David, B., and Soren, H. (2009). *GNU Octave version 3.0.1 manual: a high-level interactive language for numerical computations.* CreateSpace Independent Publishing Platform. 66

Eccles, J. C., Katz, B., and Kuffler, S. W. (1941). Nature of the "endplate potential" in curarized muscle. *Journal of Neurophysiology*, 4(5):362–387. 33

Elmqvist, D. and Quastel, D. M. (1965). A quantitative study of endplate potentials in isolated human muscle. *The Journal of physiology*, 178(3):505. 33

Gabbiani, F., Midtgaard, J., and Knopfel, T. (1994). Synaptic integration in a model of cerebellar granule cells. *Journal of Neurophysiology*, 72(2):999–1009. 30

Gasparini, S. and Magee, J. C. (2006). State-dependent dendritic computation in hippocampal CA1 pyramidal neurons. *The Journal of neuroscience*, 26(7):2088–2100. 30

Gerstner, W. and Kistler, W. M. (2002). *Spiking neuron models: Single neurons, populations, plasticity.* Cambridge university press. 39

Hansel, D. and Van Vreeswijk, C. (2002). How noise contributes to contrast invariance of orientation tuning in cat visual cortex. *The Journal of neuroscience*, 22(12):5118–5128. 30

Hebb, D. O. (1949). *The Organization of Behavior.* 33, 39

Heck, D. H., Thach, W. T., and Keating, J. G. (2007). On-beam synchrony in the cerebellum as the mechanism for the timing and coordination of movement. *Proceedings of the National Academy of Sciences*, 104(18):7658–7663. 99

Hertz, J. (1991). *Introduction to the theory of neural computation*, volume 1. Basic Books. 39

Higgs, M. H., Slee, S. J., and Spain, W. J. (2006). Diversity of gain modulation by noise in neocortical neurons: regulation by the slow afterhyperpolarization conductance. *The Journal of neuroscience*, 26(34):8787–8799. 30

Hô, N. and Destexhe, A. (2000). Synaptic Background Activity Enhances the Responsiveness of Neocortical Pyramidal Neurons. *Journal of Neurophysiology*, 84(3):1488–1496. 30

Hodgkin, A. L. and Huxley, A. F. (1952). A quantitative description of membrane current and its application to conduction and excitation in nerve. *The Journal of Physiology*, 117(4):500–544. 39, 44

Holt, G. R. and Koch, C. (1997). Shunting Inhibition Does Not Have a Divisive Effect on Firing Rates. *Neural Computation*, 9(5):1001–1013. 30, 31, 34, 63, 81

Ingham, N. J. and McAlpine, D. (2005). GABAergic inhibition controls neural gain in inferior colliculus neurons sensitive to interaural time differences. *The Journal of neuroscience*, 25(26):6187–6198. 27, 34

Kandel, E. R. (2007). *In search of memory: The emergence of a new science of mind.* W. W. Norton & Company. 19

Kandel, E. R., Schwartz, J. H., and Jessell, T. M. (2000). *Principles of neural science*, volume 4. McGraw-Hill New York. 39, 50, 57

Koch, C. (2004). *Biophysics of computation: information processing in single neurons.* Oxford university press. 39

Koch, C. and Segev, I. (1998). *Methods in neuronal modeling: from ions to networks.* MIT press. 39

London, M., Roth, A., Beeren, L., Hausser, M., and Latham, P. E. (2010). Sensitivity to perturbations in vivo implies high noise and suggests rate coding in cortex. *Nature*, 466(7302):123–127. 25, 101

Luthman, J., Hoebeek, F. E., Maex, R., Davey, N., Adams, R., De Zeeuw, C. I., and Steuber, V. (2011). STD-Dependent and Independent Encoding of Input Irregularity as Spike Rate in a Computational Model of a Cerebellar Nucleus Neuron. *Cerebellum*, 10(4):667–682. 73, 93, 104

McAdams, C. J. and Maunsell, J. H. R. (1999). Effects of attention on orientation-tuning functions of single neurons in macaque cortical area V4. *The Journal of Neuroscience*, 19(1):431–41. 27

Migliore, M., Morse, T., Davison, A., Marenco, L., Shepherd, G., and Hines, M. (2003). ModelDB. *Neuroinformatics*, 1(1):135–139. 39

Miller, K. D. and Troyer, T. W. (2002). Neural Noise Can Explain Expansive, Power-Law Nonlinearities in Neural Response Functions. *Journal of Neurophysiology*, 87(2):653–659. 30

Mitchell, S. J. and Silver, R. A. (2003). Shunting inhibition modulates neuronal gain during synaptic excitation. *Neuron*, 38(3):433–45. 30, 32, 34

Mongillo, G., Barak, O., and Tsodyks, M. (2008). Synaptic Theory of Working Memory. *Science*, 319(5869):1543–1546. 53, 104

Mountcastle, V. B., Andersen, R. A., and Motter, B. C. (1981). The influence of attentive fixation upon the excitability of the light-sensitive

neurons of the posterior parietal cortex. *The Journal of Neuroscience*, 1(11):1218–1225. 27, 28

Murphy, B. K. and Miller, K. D. (2003). Multiplicative gain changes are induced by excitation or inhibition alone. *Journal of neuroscience*, 23(31):10040–51. 34, 101

Nelson, M. (1994). A Mechanism for Neuronal Gain Control by Descending Pathways. *Neural Computation*, 6(2):242–254. 30

Oram, M. W., Wiener, M. C., Lestienne, R., and Richmond, B. J. (1999). Stochastic Nature of Precisely Timed Spike Patterns in Visual System Neuronal Responses. *Journal of Neurophysiology*, 81(6):3021–3033. 25

Oviedo, H. and Reyes, A. D. (2002). Boosting of neuronal firing evoked with asynchronous and synchronous inputs to the dendrite. *Nat Neurosci*, 5(3):261–266. 93

Pedroarena, C. M. and Schwarz, C. (2003). Efficacy and Short-Term Plasticity at GABAergic Synapses Between Purkinje and Cerebellar Nuclei Neurons. *Journal of Neurophysiology*, 89(2):704–715. 56, 71, 72, 73, 90

Person, A. L. and Raman, I. M. (2012). Purkinje neuron synchrony elicits time-locked spiking in the cerebellar nuclei. *Nature*, 481(7382):502–505. 93, 99, 103

Pouget, a. and Sejnowski, T. J. (1997). Spatial transformations in the parietal cortex using basis functions. *Journal of cognitive neuroscience*, 9(2):222–37. 28

Prescott, S. A. and De Koninck, Y. (2003). Gain control of firing rate by shunting inhibition: Roles of synaptic noise and dendritic saturation. *Proceedings of the National Academy of Sciences*, 100(4):2076–2081. 30, 33, 34

Priebe, N. J. and Ferster, D. (2002). A new mechanism for neuronal gain control (or how the gain in brains has mainly been explained). *Neuron*, 35(4):602–4. 32

Rall, W. (1962). Theory of physiological properties of dendrites. *Annals of the New York Academy of Sciences*, 96(4):1071–1092. 39

Rall, W. (1964). Theoretical significance of dendritic trees for neuronal input-output relations. *Neural theory and modeling*, pages 73–97. 49

Rancz, E. A., Ishikawa, T., Duguid, I., Chadderton, P., Mahon, S., and Hausser, M. (2007). High-fidelity transmission of sensory information by single cerebellar mossy fibre boutons. *Nature*, 450(7173):1245–1248. 72

Rieke, F. (1999). *Spikes: exploring the neural code.* MIT press. 25

Rothman, J. S., Cathala, L., Steuber, V., and Silver, R. A. (2009). Synaptic depression enables neuronal gain control. *Nature*, 457(7232):1015–1018. 19, 20, 30, 33, 35, 36, 62, 63, 64, 67, 71, 102

Sabbatini, R. (2003). Neurons and synapses: The history of its discovery. *Brain & Mind Magazine*, 17. 39, 40

Salinas, E. and Abbott, L. F. (1995). Transfer of coded information from sensory to motor networks. *The Journal of neuroscience : the official journal of the Society for Neuroscience*, 15(10):6461–74. 28

Salinas, E. and Thier, P. (2000). Gain modulation: A major computational principle of the central nervous system. *Neuron*, 27:15–21. 27, 29

Saviane, C. and Silver, R. A. (2006). Fast vesicle reloading and a large pool sustain high bandwidth transmission at a central synapse. *Nature*, 439(7079):983–987. 33, 72

Schutter, E. D. (2009). *Computational modeling methods for neuroscientists.* The MIT Press. 39

Shin, S.-L., Hoebeek, F. E., Schonewille, M., De Zeeuw, C. I., Aertsen, A., and De Schutter, E. (2007). Regular patterns in cerebellar Purkinje cell simple spike trains. *PloS one*, 2(5):e485. 55, 56, 71, 72, 73, 89, 90

Shu, Y., Hasenstaub, A., Badoual, M., Bal, T., and McCormick, D. A. (2003). Barrages of synaptic activity control the gain and sensitivity of cortical neurons. *The Journal of neuroscience*, 23(32):10388–10401. 30

Silver, R. A. (2010). Neuronal arithmetic. *Nature Reviews, Neuroscience*, 11(7):474–89. 25, 31, 35, 36, 102

Softky, W. R. (1995). Simple codes versus efficient codes. *Current Opinion in Neurobiology*, 5(2):239–247. 25

Sterratt, D., Graham, B., Gillies, A., and Willshaw, D. (2011). *Principles of computational modelling in neuroscience.* Cambridge University Press. 39

Steuber, V. and Jaeger, D. (2013). Modeling the generation of output by the cerebellar nuclei. *Neural Networks*, 47(0):112–119. 71, 104

Steuber, V., Schultheiss, N. W., Silver, R. A., De Schutter, E., and Jaeger, D. (2011). Determinants of synaptic integration and heterogeneity in rebound firing explored with data-driven models of deep cerebellar nucleus cells. *Journal of Computational Neuroscience*, 30(3):633–58. 20, 34, 63, 72, 74

Tamás, G., Szabadics, J., and Somogyi, P. (2002). Cell type-and subcellular position-dependent summation of unitary postsynaptic potentials in neocortical neurons. *The Journal of neuroscience*, 22(3):740–747. 30

Tiesinga, P. H. E., José, J. V., and Sejnowski, T. J. (2000). Comparison of current-driven and conductance-driven neocortical model neurons with Hodgkin-Huxley voltage-gated channels. *Physical Review E*, 62(6):8413–8419. 30

Tovee E. T. Azzopardi, P., M. J. R. (1994). Translation invariance in the responses to faces of single neurons in the temporal visual cortical areas of the alert macaque. *Journal of Neurophysiology*, 72(3):1049–1060. 27

Treue, S. and Martínez Trujillo, J. C. (1999). Feature-based attention influences motion processing gain in macaque visual cortex. *Nature*, 399(6736):575–9. 27

Trussell, L. O. and Fischbach, G. D. (1989). Glutamate receptor desensitization and its role in synaptic transmission. *Neuron*, 3(2):209–218. 33

Varela, J. A., Sen, K., Gibson, J., Fost, J., Abbott, L. F., and Nelson, S. B. (1997). A Quantitative Description of Short-Term Plasticity at Excitatory Synapses in Layer 2/3 of Rat Primary Visual Cortex. *The Journal of Neuroscience*, 17(20):7926–7940. 53, 55, 64

Zipser, D. and Andersen, R. A. (1988). A back-propagation programmed network that simulates response properties of a subset of posterior parietal neurons. *Nature*, 331(6158):679–684. 19, 28, 29

Publications

- **Dimitris Bampasakis**, Reinoud Maex, Neil Davey, and Volker Steuber (2014). Determinants of gain modulation enabled by short-term depression at an inhibitory cerebellar synapse. BMC Neuroscience 15, P11. **//Oral presentation**

- **Dimitris Bampasakis**, Reinoud Maex, Neil Davey, and Volker Steuber (2014). Multiplicative gain modulation arising from inhibitory synaptic plasticity in the cerebellar nuclei. Frontiers in Systems Neuroscience. **//Poster presentation**

- **Dimitris Bampasakis**, Reinoud Maex, Neil Davey, and Volker Steuber (2013). Short-term depression of inhibitory Purkinje cell synapses enhances gain modulation in the cerebellar nuclei. BMC Neuroscience 14, P374. **//Poster presentation**

- Hugo Cornelis, **Dimitris Bampasakis**, Volker Steuber, James M. Bower (2013). Interoperability in the GENESIS 3.0 Software Federation: the NEURON Simulator as an Example. BMC Neuroscience 14, P33. **//Poster presentation**

BMC Neuroscience

ORAL PRESENTATION

Open Access

Determinants of gain modulation enabled by short-term depression at an inhibitory cerebellar synapse

Dimitris Bampasakis[1*], Reinoud Maex[2], Neil Davey[1], Volker Steuber[1]

From The Twenty Third Annual Computational Neuroscience Meeting: CNS*2014
Québec City, Canada. 26-31 July 2014

Neurons adapt rapidly the slope, also known as gain, of their input-output function to time-varying conditions. Gain modulation is a prominent mechanism in many brain processes, such as auditory processing and attention scaling of orientation tuning curves. It is known to amplify neuronal signals, prevent firing saturation, and play a key role in coordinate transformation [1].

Synaptic short-term depression (STD) at the excitatory synapse from mossy fibres (MFs) to granule cells in the cerebellum has previously been found to introduce a gain change, and enhance inhibition-mediated gain modulation [2]. Similar results were discovered for STD at the inhibitory synapse from Purkinje cells (PCs) to cerebellar nucleus (CN) neurons, where STD modulates gain and enhances excitation-mediated gain modulation [3]. In both cases – whether STD is applied at the excitatory or inhibitory synapse, respectively – the non-linearity introduced by STD in the relationship between input firing rate and average conductance, was found to underlie the effects of STD.

We use a multi-compartment model of a cerebellar nucleus neuron [4] to understand how STD at an inhibitory synapse can add a multiplicative component in the transformation performed by excitatory input. To do so, we use input from PCs, applied at an inhibitory synapse with STD, and excitatory input from MFs, while changing the level of STD by manipulating the presynaptic release probability (R) [5]. We find that gain modulation resulting from the introduction of STD increases with the extent of depression. To further our understanding, we investigate the effects of STD using synchronous input, regular input, and their combination. We find that the multiplicative

component introduced by STD remains, but varies in value for different input conditions. Moreover, we present a detailed analysis of how a non-linear mapping between input spike rate and synaptic conductance can result in multiplicative operations.

Authors' details
[1]Science and Technology Research Institute, University of Hertfordshire, Hatfield AL10 9AB, UK. [2]Department of Cognitive Sciences, École Normale Supérieure, Paris 75005, France.

References
1. Silver RA: **Neuronal arithmetic.** *Nature Reviews Neuroscience* 2010, **11**:474-489.
2. Rothman JS, Cathala L, Steuber V, Silver RA: **Synaptic depression enables neuronal gain control.** *Nature* 2009, **457**:1015-1018.
3. Bampasakis D, Maex R, Davey N, Steuber V: **Short-term depression of inhibitory Purkinje cell synapses enhances gain modulation in the cerebellar nuclei.** *BMC Neuroscience* 2013, **14**:374.
4. Steuber V, Schultheiss NW, Silver RA, De Schutter E, Jaeger D: **Determinants of synaptic integration and heterogeneity in rebound firing explored with data-driven models of deep cerebellar nucleus cells.** *Journal of Computational Neuroscience* 2011, **3(3)**:633-58.
5. Shin SL, Hoebeek F, Schonewille M, De Zeeuw CI, Aertsen A, De Schutter E: **Regular patterns in cerebellar Purkinje cell simple spike trains.** *PloS One* 2007, **2(5)**:e485.

* Correspondence: d.bampasakis@herts.ac.uk
[1]Science and Technology Research Institute, University of Hertfordshire, Hatfield AL10 9AB, UK
Full list of author information is available at the end of the article

BMC
Neuroscience

POSTER PRESENTATION   **Open Access**

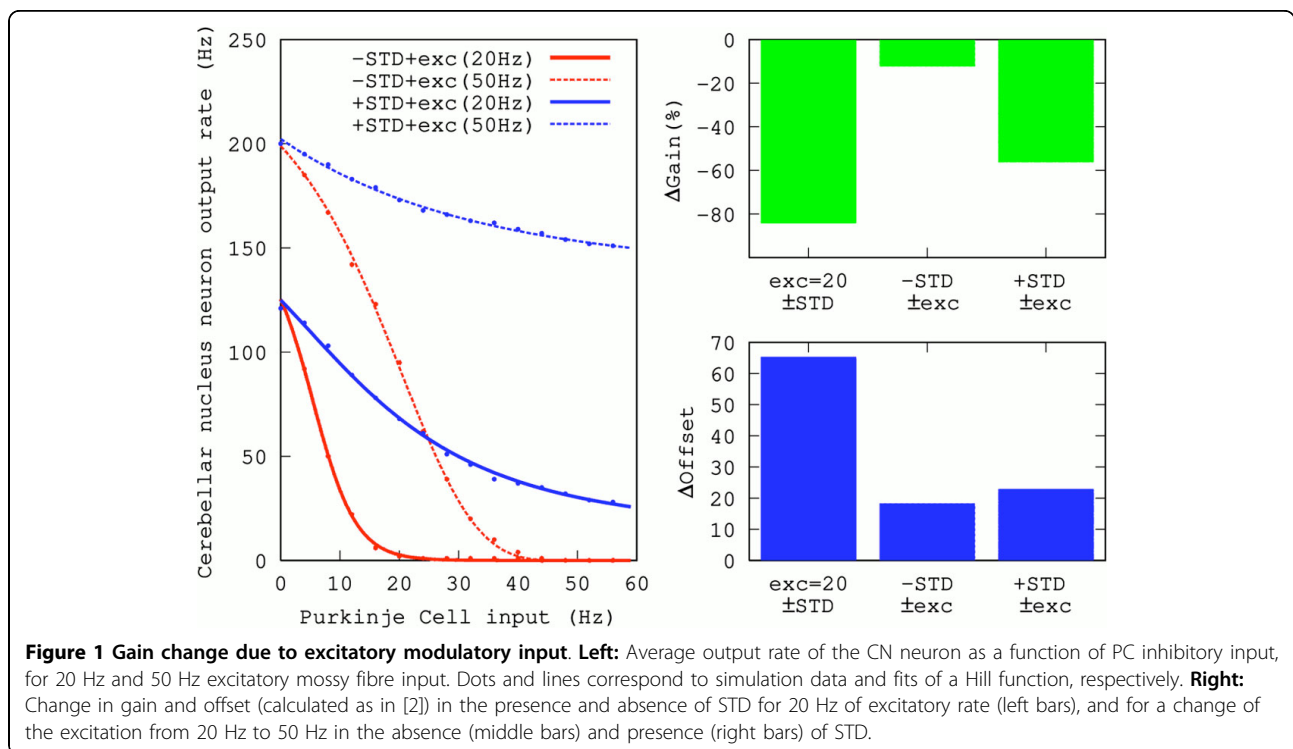# Short-term depression of inhibitory Purkinje cell synapses enhances gain modulation in the cerebellar nuclei

Dimitris Bampasakis[1*], Reinoud Maex[2], Neil Davey[1], Volker Steuber[1]

From Twenty Second Annual Computational Neuroscience Meeting: CNS*2013
Paris, France. 13-18 July 2013

Information in neurons can be encoded by their action potential rate, thus making the transformation of input to output rate, the input-output (I-O) relationship, a core computational function. Introduction of a second input, often called modulatory input, can modify this I-O relationship in ways that correspond to different arithmetic operations [1]. Here, we examine the modulation of the slope of the I-O relationship, also referred to as gain modulation.

Gain modulation can be based on a wide variety of biophysical mechanisms, with short-term depression (STD) of excitatory synapses being one of them [2].

Figure 1 Gain change due to excitatory modulatory input. **Left:** Average output rate of the CN neuron as a function of PC inhibitory input, for 20 Hz and 50 Hz excitatory mossy fibre input. Dots and lines correspond to simulation data and fits of a Hill function, respectively. **Right:** Change in gain and offset (calculated as in [2]) in the presence and absence of STD for 20 Hz of excitatory rate (left bars), and for a change of the excitation from 20 Hz to 50 Hz in the absence (middle bars) and presence (right bars) of STD.

* Correspondence: d.bampasakis@herts.ac.uk
[1]Science and Technology Research Institute, University of Hertfordshire,
Hatfield AL10 9AB, UK

BMC
Neuroscience

POSTER PRESENTATION

Open Access

Interoperability in the GENESIS 3.0 Software Federation: the NEURON Simulator as an Example

Hugo Cornelis[1*], Dimitris Bampasakis[3], Volker Steuber[3], James M Bower[1,2]

The idea of "interoperability" of neuroscience modeling software was instigated by the problems associated with incomplete model specifications in published papers and incremental model extensions through research projects across laboratories. Cannon et al. [1] defined interoperability as "all mechanisms that allow two or more simulators to use the same model description or to collaborate by evaluating different parts of a large neural model". As an example, the adoption of common declarative model definition languages such as *SBML*, *NeuroML*, and *NineML*, allows to simulate the same model on different simulator environments. Run-time interoperability allows different simulators to compute different aspects of the same model at run-time either by direct coupling via simulator script languages, indirect coupling via interpreted languages, or coupling via object oriented frameworks (see [2] for details).

The Computational Biology Initiative (CBI) federated software architecture is a software architecture that transparently supports both interoperability and "extensibility" for model building, simulation, and result analysis. It is a modular meta-framework for software development that integrates all the functions necessary for a fully functioning simulator. The modular nature of the CBI Architecture provides several advantages for multiple independent contributions to software development including: (1) Reduction in complexity of individual simulator components when compared to the complexity of a complete simulator, (2) Easy removal or replacement of unnecessary or obsoleted components, and (3) Clear delineation of the development scope of new components.

The CBI Architecture is designed to support alternative paradigms of interoperability and extensibility through the provision of logical relationships between its modules. The definition of a common information exchange reference model allows software modules to automatically interpret the information exchanged meaningfully and accurately in order to produce useful results as defined by end users such that any appropriately configured software component or application can be incorporated into the simulator.

GENESIS 3.0 (G-3) is a major reconfiguration and update of the GENESIS simulation system. G-3 is the first neural simulator to comply with the modular design of the CBI Architecture. It embodies many software components, each of which has been developed in full isolation. These include the **Model Container** that efficiently stores a representation of a model in computer memory and has simple bindings to the NeuroML and NineML declarative modeling languages, and **Heccer**: A fast compartmental solver based on the GENESIS *hsolve* object that can be instantiated from C, Python, Perl or other scripting languages. The **NS-SLI** is the G-3 component that provides backward compatibility for the GENESIS-2 SLI.

In this presentation we report on our recent efforts to reconfigure the NEURON simulator as an independent CBI compliant software component and to integrate its scripting interfaces with other CBI compliant software components of the GENESIS 3.0 neural simulation framework. The integration of selected aspects of the NEURON simulator into G-3 will allow to seamlessly integrate HOC model components with G-2 or G-3 model components. Employed in this way, the modular paradigm of the CBI Architecture supports interoperability by facilitating the functional integration of otherwise independent applications.

* Correspondence: hugo.cornelis@gmail.com
[1]University of Texas Health Science Center, San Antonio, Texas, 78245, USA
Full list of author information is available at the end of the article

BioMed Central